Studying the $b \to s\ell^+\ell^-$ anomalies and $(g-2)_\mu$ in R-parity violating MSSM framework with the inverse seesaw mechanism

Min-Di Zheng[†] and Hong-Hao Zhang[*]

School of Physics, Sun Yat-Sen University, Guangzhou 510275, China

(Received 9 June 2021; accepted 29 November 2021; published 20 December 2021)

Inspired by the recent experimental results which show deviations from the standard model predictions of $b \to s\ell^+\ell^-$ transitions, we study the R-parity violating minimal supersymmetric standard model extended by the inverse seesaw mechanism. The trilinear R-parity violating terms, together with the chiral mixing of sneutrinos, induce the loop contributions to the $b \to s\ell^+\ell^-$ anomaly. We study the parameter space of the single-parameter scenario $C_{9,\mu}^{\rm NP} = -C_{10,\mu}^{\rm NP} = C_{\rm V}$ and the double-parameter scenario $(C_{\rm V}, C_{\rm U})$, respectively, constrained by other experimental data such as $B_s - \bar{B}_s$ mixing, $B \to X_s\gamma$ decay, the lepton flavor violating decays, etc. Both the single-parameter and the double-parameter scenario can resolve the long existing muon anomalous magnetic moment problem, as well, and allow the anomalous $t \to cg$ process to reach the sensitivity at the Future Circular hadron-hadron Collider.

DOI: 10.1103/PhysRevD.104.115023

I. INTRODUCTION

In recent years, several hints of new physics (NP) beyond the standard model (SM) have shown up, such as $R_{K^{(*)}} = \mathcal{B}(B \to K^{(*)}\mu^+\mu^-)/\mathcal{B}(B \to K^{(*)}e^+e^-)$ on the transitions of $b \to s\ell^+\ell^-$ ($\ell = e,\ \mu$), which exhibits very attractive anomalies. In particular, the measurement of R_K by the LHCb Collaboration has just been updated with the full run II data, as $R_K = 0.846^{+0.042+0.013}_{-0.039-0.012}$ in the q^2 bin $[1.1, 6]$ GeV^2 [1], which is much more precise than the previous data $R_K = 0.846^{+0.060+0.016}_{-0.054-0.014}$ [2], giving rise to discrepancy with the SM value changing from the preceding 2.5σ to 3.1σ. The recent measurements of R_{K^*} by LHCb give $R_{K^*} = 0.66^{+0.11}_{-0.07} \pm 0.03$ at the $[0.045, 1.1]$ GeV^2 bin and $R_{K^*} = 0.69^{+0.11}_{-0.07} \pm 0.05$ at the $[1.1, 6]$ GeV^2 bin, showing a 2.1σ deviation at the low q^2 region and a 2.5σ deviation at the high region, respectively [3]. The $R_{K^{(*)}}$ results by the Belle Collaboration [4,5] show consistency with the SM predictions, although the results have sizeable experimental error bars. Besides, there are also other anomalies in the $b \to s\ell^+\ell^-$ transition, for instance, the angular observable P_5' anomaly of the $B \to K^*\mu^+\mu^-$ decay persists with the new data [6] when compared with the run I results [7–12]. All of these anomalies may indicate the NP that breaks lepton flavor universality (LFU).

We know that each single anomaly above cannot be regarded as the conclusive evidence of NP. However, it is interesting that nearly all of these anomalies can be explained simultaneously with the four-Fermi operators in the model-independent global fit [13–36]. In light of the new measurement of R_K [1], there are already some new fit results updated [14,23–36]. For the discussion of the global fit, the related Lagrangian of the low energy effective field theory is given by

$$\mathcal{L}_{\rm eff} = \frac{4G_F}{\sqrt{2}}\eta_t \sum_i C_i \mathcal{O}_i + \text{H.c.}, \tag{1.1}$$

where the Cabibbo–Kobayashi–Maskawa (CKM) factor $\eta_t \equiv K_{tb}K_{ts}^*$. The main operators for the anomaly explanations are

$$\mathcal{O}_9 = \frac{e^2}{16\pi^2}(\bar{s}\gamma_\mu P_L b)(\bar{\ell}\gamma^\mu \ell),$$
$$\mathcal{O}_{10} = \frac{e^2}{16\pi^2}(\bar{s}\gamma_\mu P_L b)(\bar{\ell}\gamma^\mu\gamma_5 \ell), \tag{1.2}$$

where $P_L = (1-\gamma_5)/2$ is the left-handed (LH) chirality projector and the Wilson coefficients are $C_{9(10)} = C_{9(10)}^{\rm SM} + C_{9(10)}^{\rm NP}$. In this work, we adopt the following unified form of fit scenarios:

$$C_{9,\mu}^{\rm NP} = C_{\rm V} + C_{\rm U}, \qquad C_{10,\mu}^{\rm NP} = -C_{\rm V},$$
$$C_{9,e}^{\rm NP} = C_{\rm U}, \qquad C_{10,e}^{\rm NP} = 0, \tag{1.3}$$

[*]Corresponding author.
zhh98@mail.sysu.edu.cn
[†]zhengmd5@mail.sysu.edu.cn

where V denotes the contributions only of the $\mu^+\mu^-$ channel and U denotes LFU contributions. The first scenario, called scenario A here, requires $C_{\rm U} = 0$ to realize the single-parameter scenario $C_{9,\mu}^{\rm NP} = -C_{10,\mu}^{\rm NP}$, in fact. We adopt the fit result $-0.46 < C_{\rm V} < -0.32$, which conforms to the rare B-meson decays at the 1σ level in Ref. [28]. Except for the new R_K measurement [1], authors in Ref. [28] have also considered other series of new experimental results, such as the new angular analyses of $B^0 \to K^{*0}\mu^+\mu^-$ [6] and $B^\pm \to K^{*\pm}\mu^+\mu^-$ [37], the updated branching ratio measurement of $B_s \to \phi\mu^+\mu^-$ [38] that confirms the previous tension [39] with the SM prediction, as well as the recent results of $B_s \to \mu^+\mu^-$ from CMS [40] and LHCb [41,42]. For the case of $C_{\rm U} \neq 0$, named as scenario B, we also utilize the fit regions in Ref. [28] with the best fit point, $(C_{\rm V}, C_{\rm U}) \approx (-0.34, -0.32)$.

After these results of the model-independent analyses are obtained, the imperative work is to find the concrete NP models which can conform to them. Both scenarios A and B have been implemented in the R-parity violating minimal supersymmetric standard model (MSSM) [43–48]. When masses of sneutrinos/sd-quarks are sufficiently heavy or there is a cancellation in the penguin contribution [46], scenario B turns into scenario A.

More than the R-parity violating MSSM, the seesaw mechanism [49–55] is also researched for the explanation of $b \to s\ell^+\ell^-$ disparities in the supersymmetric (SUSY) models [56], the two-Higgs doublet [57,58], and other frameworks (see, e.g., Refs. [59–73]). The seesaw mechanism is one of the most attractive methods to generate the neutrino masses in accord with the conclusive evidence of neutrino oscillations [74], as one type of seesaw mechanism, the inverse seesaw [75,76], can give a $\mathcal{O}(1)$ neutrino Yukawa coupling Y_ν. The relative large Y_ν implicates that the admixture between LH neutrino superfields and right-handed (RH) or extra singlet superfields is not negligible. Therefore, it is meaningful to study the chiral mixings of (s)neutrinos in the MSSM framework extended by both inverse seesaw mechanisms and the tree-level trilinear R-parity violating (RPV) terms, and then all chiral parts of (s)neutrinos more than LH ones can interact with (s)quarks. This new combination is naturally reasonable [77–79] and has never been studied in the $b \to s\ell^+\ell^-$ anomalies to our knowledge.

The recent experimental results of $R(D^{(*)}) = \mathcal{B}(B \to D^{(*)}\tau\nu)/\mathcal{B}(B \to D^{(*)}\ell\nu)$ in the charged current $b \to c\tau\nu$ from *BABAR* [80,81], Belle [82–85], and LHCb [86–88] have been averaged by the Heavy Flavor Averaging Group [89], and also show the tension with the average of SM predictions [90–93] and the recent new SM results [94–99]. While the new measurements of $R(D^{(*)})$ from Belle using the semileptonic tagging method, such as the latest results with the data sample of 772×10^6 $B\bar{B}$ pairs, are already in good agreement with SM predictions, Belle combined results are consistent with SM predictions within 1.6σ [100]. Given this, in this work we do not investigate $R(D^{(*)})$ for the moment.

The clues of LFU violation exist not only in B-meson decays but also in other processes, such as the muon anomalous magnetic moment problem, which has existed for several decades. The measurement of $a_\mu = (g-2)_\mu$ by Fermilab [101–103] presents the 3.3σ deviation as greater than the SM prediction [104],[1] and agrees with the previous Brookhaven E821 experiment [114]. The combined deviation average of the two experiments, $\Delta a_\mu = a_\mu^{\rm exp} - a_\mu^{\rm SM} = (2.51 \pm 0.59) \times 10^{-9}$, shows the increased tension at the significant 4.2σ level, and this is a growing motivation of NP. For the electron anomalous magnetic moment, there is a negative 2.4σ discrepancy between the measurement [115] and the SM prediction [116], $\Delta a_e = a_e^{\rm exp} - a_e^{\rm SM} = (-8.7 \pm 3.6) \times 10^{-13}$, due to the new measurement of the fine structure constant in Ref. [117].[2] There are plenty of articles discussing the $(g-2)_\mu$ problem in the SUSY framework (e.g., see Refs. [48,120–169]). In this work, we will investigate whether the parameter space for the explanation of $b \to s\ell^+\ell^-$ anomalies can be in accordance with the deviation Δa_μ, and then we will discuss the NP effects on a_e.

Our paper is organized as follows. At first, the new model in this work is introduced in Sec. II. Then, in Sec. III, the one-loop contributions to the $b \to s\ell^+\ell^-$ transition in this model are scrutinized and we emphasize the main contributions to explain the $b \to s\ell^+\ell^-$ anomaly in our parameter scheme. We discuss NP contributions to $(g-2)_\ell$ and other related constraints in Sec. IV, followed by the numerical results and discussions in Sec. V. Our conclusions are presented in Sec. VI.

II. THE MODEL

The model considered in this work is R-parity violating MSSM with the inverse seesaw mechanism, called RPV-MSSMIS here, and the superpotential is expressed by

$$\mathcal{W} = \mathcal{W}_{\rm MSSM} + Y_\nu^{ij}\hat{R}_i\hat{L}_j\hat{H}_u + M_R^{ij}\hat{R}_i\hat{S}_j + \frac{1}{2}\mu_S^{ij}\hat{S}_i\hat{S}_j + \lambda'_{ijk}\hat{L}_i\hat{Q}_j\hat{D}_k, \tag{2.1}$$

[1] A recent calculation of the hadronic vacuum polarization (HVP) [105] weakens the discrepancy between the experiment and SM prediction of a_μ, while it shows the tension with the R-ratio determinations [106–109]. Even the large HVP contribution can account for the measurement of a_μ, as there exists the tension within the electroweak (EW) fit [110–113]. We do not consider this HVP result here but consider the preceding review of various SM results [104].

[2] Another new measurement of the fine structure constant [118] differs by more than 5σ to the previous one [117] and affects the deviation Δa_e to a positive 1.6σ level [119]. The NP hint search in a_e still expects more experimental researches and we focus on a_μ anomaly explanations in this work.

where the generation indices are i, j, $k = 1, 2, 3$, while the color ones are omitted. All the repeated indices are defaulted to be summed over unless otherwise stated. Here the superpotential of the MSSM [170,171] is expressed as

$$\mathcal{W}_{\rm MSSM} = \mu \hat{H}_u \hat{H}_d + Y_u^{ij} \hat{U}_i \hat{Q}_j \hat{H}_u - Y_d^{ij} \hat{D}_i \hat{Q}_j \hat{H}_d - Y_e^{ij} \hat{E}_i \hat{L}_j \hat{H}_d. \tag{2.2}$$

In the RPV-MSSMIS, MSSM superfields are extended by three generations of pairs of SM singlet superfields, $\hat{R}_i$ and $\hat{S}_i$. The neutral parts of two Higgs doublet superfields, $\hat{H}_u = (\hat{H}_u^+, \hat{H}_u^0)^T$ and $\hat{H}_d = (\hat{H}_d^0, \hat{H}_d^-)^T$, acquire the nonzero vacuum expectation values, $\langle \hat{H}_u^0 \rangle = v_u$ and $\langle \hat{H}_d^0 \rangle = v_d$, respectively, leading to the mixing angle $\beta = \tan^{-1}(v_u/v_d)$. The tree-level trilinear RPV coupling $\lambda'_{ijk} \hat{L}_i \hat{Q}_j \hat{D}_k$ can be added for $\hat{L}_i$ sharing the same SM quantum number with $\hat{H}_d$. It is necessary to point out that the RPV superpotential terms like $\lambda'_{ijk} \hat{L}_i \hat{Q}_j \hat{D}_k$, $\lambda_{ijk} \hat{L}_i \hat{L}_j \hat{E}_k$, $\lambda''_{ijk} \hat{U}_i \hat{D}_j \hat{D}_k$, and $\mu_i \hat{L}_i \hat{H}_u$ are all, in principle, allowed for the SM gauge invariance if there are no extra symmetries. Here we only consider the term $\lambda'_{ijk} \hat{L}_i \hat{Q}_j \hat{D}_k$, connecting the quark sector with the lepton sector, without the pure-quark term $\lambda''_{ijk} \hat{U}_i \hat{D}_j \hat{D}_k$ or the purely lepton interaction $\lambda_{ijk} \hat{L}_i \hat{L}_j \hat{E}_k$. This is an attempt to avoid the probable disastrously rapid proton decay [172,173] that occurs when there are nonzero parameters λ' and λ'' simultaneously and the strong collider constraints on the lightest sneutrino mass when λ' and λ both exist [174–184]. The bilinear term $\mu_i \hat{L}_i \hat{H}_u$ is also allowed, but we exclude it in order to avoid the extra contributions to neutrino masses [185]. With the scalar components of Higgs doublet superfields denoted by H_u and H_d, and squarks and sleptons denoted by "~", the soft supersymmetry breaking Lagrangian is given by

$$\begin{aligned} -\mathcal{L}^{\rm soft} = & -\mathcal{L}^{\rm soft}_{\rm MSSM} + (m_{\tilde{R}}^2)_{ij} \tilde{R}_i^* \tilde{R}_j + (m_{\tilde{S}}^2)_{ij} \tilde{S}_i^* \tilde{S}_j \\ & + (A_\nu Y_\nu)_{ij} \tilde{R}_i^* \tilde{L}_j H_u + B_{M_R}^{ij} \tilde{R}_i^* \tilde{S}_j + \frac{1}{2} B_{\mu_S}^{ij} \tilde{S}_i \tilde{S}_j, \end{aligned} \tag{2.3}$$

where $\mathcal{L}^{\rm soft}_{\rm MSSM}$ corresponds to the MSSM part [170,171]. It should be mentioned that MSSM and singlet neutrino sectors are all at low scale (around 1 TeV) in this work, so some terms in the most general superpotential and soft breaking Lagrangian are already or will be eliminated *ad hoc* for the phenomenological consideration.

As to the three terms following $\mathcal{W}_{\rm MSSM}$ in Eq. (2.1), which give the neutrino mass spectrum at tree level, the 9×9 mass matrix of the neutrino in the (ν, R, S) basis is given by

$$\mathcal{M}_\nu = \begin{pmatrix} 0 & m_D^T & 0 \\ m_D & 0 & M_R \\ 0 & M_R^T & \mu_S \end{pmatrix}, \tag{2.4}$$

in which $m_D = \frac{1}{\sqrt{2}} v_u Y_\nu^T$. The μ_S parameter can be obtained by

$$\mu_S = (m_D^T)^{-1} M_R U_{\rm PMNS} m_\nu^{\rm diag} U_{\rm PMNS}^T M_R^T m_D^{-1}, \tag{2.5}$$

where $\mu_S \ll m_D < M_R$. The diagonalized neutrino mass $\mathcal{M}_\nu^{\rm diag}$ in a physics basis, containing the three-light-generation part $m_\nu^{\rm diag}$ in Eq. (2.5), is given by $\mathcal{M}_\nu^{\rm diag} = \mathcal{V} \mathcal{M}_\nu \mathcal{V}^T$. Here, embedded in the whole 9×9 mixing matrix $\mathcal{V}^T$, the 3×3 light-generation sector $\mathcal{V}_{3\times3}^T$ should approximate the PMNS matrix $U^{\rm PMNS}$ [74,186].

We then turn to the sneutrino mass square matrix in the $(\tilde{\nu}_L^{\mathcal{I}(R)}, \tilde{R}^{\mathcal{I}(R)}, \tilde{S}^{\mathcal{I}(R)})$ basis, which is expressed as

$$\mathcal{M}^2_{\tilde{\nu}^{\mathcal{I}(R)}} = \begin{pmatrix} m_{\tilde{L}'}^2 & (A_\nu - \mu \cot\beta) m_D^T & m_D^T M_R \\ (A_\nu - \mu \cot\beta) m_D & m_{\tilde{R}}^2 + M_R M_R^T + m_D m_D^T & \pm M_R \mu_S + B_{M_R} \\ M_R^T m_D & \pm \mu_S M_R^T + B_{M_R}^T & m_{\tilde{S}}^2 + \mu_S^2 + M_R^T M_R \pm B_{\mu_S} \end{pmatrix}, \tag{2.6}$$

where the "$\pm$" above expresses the CP-even and CP-odd masses, where CP odd is denoted by $\mathcal{I}$ and CP even is denoted by $\mathcal{R}$. The soft mass $m_{\tilde{L}'}^2 = m_{\tilde{L}}^2 + \frac{1}{2} m_Z^2 \cos 2\beta + m_D m_D^T$ can be regarded as one whole input, where $m_{\tilde{L}}^2$ is the soft mass square of $\tilde{L}$ in $\mathcal{L}^{\rm soft}_{\rm MSSM}$. The CP-even and CP-odd masses can be nearly the same for tiny μ_S and relatively small B_{μ_S} [187]. Besides, the value of $m_{\tilde{S}}^2$ is set to be zero here. Thus, the approximate form is provided as [188]

$$\mathcal{M}^2_{\tilde{\nu}^{\mathcal{I}(R)}} \approx \begin{pmatrix} m_{\tilde{L}'}^2 & (A_\nu - \mu \cot\beta) m_D^T & m_D^T M_R \\ (A_\nu - \mu \cot\beta) m_D & m_{\tilde{R}}^2 + M_R M_R^T + m_D m_D^T & B_{M_R} \\ M_R^T m_D & B_{M_R}^T & M_R^T M_R \end{pmatrix}. \tag{2.7}$$

In the following, we adopt this particular structure and then the mixing matrices $\tilde{\mathcal{V}}^{\mathcal{I}(R)}$, which diagonalize sneutrino mass square matrices by $\tilde{\mathcal{V}}^{\mathcal{I}(R)}\mathcal{M}^2_{\tilde{\nu}^{\mathcal{I}(R)}}\tilde{\mathcal{V}}^{\mathcal{I}(R)\dagger} = (\mathcal{M}^2_{\tilde{\nu}^{\mathcal{I}(R)}})^{\rm diag}$, are also the same whether CP even or odd. All the $\tilde{\mathcal{V}}^{\mathcal{R}}$ and the physical mass $m_{\tilde{\nu}^{\mathcal{R}}}$ can be expressed as $\tilde{\mathcal{V}}^{\mathcal{I}}$ and $m_{\tilde{\nu}^{\mathcal{I}}}$, respectively, in the rest of the paper. With respect to charged sleptons, the LH sector element is given by $m^2_{\tilde{L}'} + m^2_l - m_D m_D^T - m_W^2 \cos 2\beta$.

Afterwards, we discuss the last term of the superpotential. For the superpotential term $\lambda'_{ijk}\hat{L}_i\hat{Q}_j\hat{D}_k$, the corresponding Lagrangian in the flavor basis is obtained as

$$\mathcal{L}_{\rm LQD} = \lambda'_{ijk}(\tilde{\nu}_{Li}\bar{d}_{Rk}d_{Lj} + \tilde{d}_{Lj}\bar{d}_{Rk}\nu_{Li} + \tilde{d}^*_{Rk}\bar{\nu}^c_{Li}d_{Lj} - \tilde{l}_{Li}\bar{d}_{Rk}u_{Lj} - \tilde{u}_{Lj}\bar{d}_{Rk}l_{Li} - \tilde{d}^*_{Rk}\bar{l}^c_{Li}u_{Lj}) + \text{H.c.}, \quad (2.8)$$

where "c" indicates the charge conjugated fermions. Then in the context of mass eigenstates for the down quarks and charged leptons, the Lagrangian above with other fields $\tilde{\nu}_L$, ν_L, and u_L (aligned with $\tilde{u}_L$), rotated to mass eigenstates by mixing matrices $\tilde{\mathcal{V}}^{\mathcal{I}(R)}$, $\mathcal{V}$, and K, respectively, is given by

$$\mathcal{L}'_{\rm LQD} = \lambda'^{\mathcal{I}(R)}_{vjk}\tilde{\nu}_v\bar{d}_{Rk}d_{Lj} + \lambda'^{\mathcal{N}}_{vjk}(\tilde{d}_{Lj}\bar{d}_{Rk}\nu_v + \tilde{d}^*_{Rk}\bar{\nu}^c_v d_{Lj}) - \tilde{\lambda}'_{ilk}(\tilde{l}_{Li}\bar{d}_{Rk}u_{Ll} + \tilde{u}_{Ll}\bar{d}_{Rk}l_{Li} + \tilde{d}^*_{Rk}\bar{l}^c_{Li}u_{Ll}) + \text{H.c.}, \quad (2.9)$$

where all the fields are represented by the mass eigenstates. Concretely, ν_v and $\tilde{\nu}_v$ are in the mass eigenstate with the index $v = 1, 2, \ldots 9$ and the three neo-λ' terms are deduced as $\lambda'^{\mathcal{I}(R)}_{vjk} = \lambda'_{ijk}\tilde{\mathcal{V}}^{\mathcal{I}(R)*}_{vi}$, $\lambda'^{\mathcal{N}}_{vjk} = \lambda'_{ijk}\mathcal{V}^*_{vi}$, and $\tilde{\lambda}'_{ilk} = \lambda'_{ijk}K^*_{lj}$. In the following, we call the diagrams including these λ' couplings "λ' diagrams," otherwise we call them "non-λ' diagrams."

By the end of this section, we should mention the chargino and neutralino mass matrices in the MSSM sector of this model. The chargino mass matrix is [171]

$$\mathcal{M}_{\chi^\pm} = \begin{pmatrix} M_2 & \sqrt{2}m_w \sin\beta \\ \sqrt{2}m_w\cos\beta & \mu \end{pmatrix}, \quad (2.10)$$

where the parameter M_2 is the wino mass and μ is related to the Higgsino mass. The mixing matrices V and U diagonalize $\mathcal{M}_{\chi^\pm}$ by $U^*\mathcal{M}_{\chi^\pm}V^\dagger = \mathcal{M}^{\rm diag}_{\chi^\pm}$. As for the neutralino mass matrix $\mathcal{M}_{\chi^0}$ in the basis $(\tilde{B}, \tilde{W}^3, \tilde{H}^0_d, \tilde{H}^0_u)^T$ [171],

$$\mathcal{M}_{\chi^0} = \begin{pmatrix} M_1 & 0 & -\frac{ev_d}{2\cos\theta_W} & \frac{ev_u}{2\cos\theta_W} \\ 0 & M_2 & \frac{ev_d}{2\sin\theta_W} & -\frac{ev_u}{2\sin\theta_W} \\ -\frac{ev_d}{2\cos\theta_W} & \frac{ev_d}{2\sin\theta_W} & 0 & -\mu \\ \frac{ev_u}{2\cos\theta_W} & -\frac{ev_u}{2\sin\theta_W} & -\mu & 0 \end{pmatrix}, \quad (2.11)$$

with M_1 being the bino mass and θ_W being the weak mixing angle, and it is diagonalized by $N\mathcal{M}_{\chi^0}N^T = \mathcal{M}^{\rm diag}_{\chi^0}$.

III. $b \to s\ell^+\ell^-$ PROCESS IN THE RPV-MSSMIS

In the RPV-MSSMIS, the tree-level diagram of the $b \to s\ell^+\ell^-$ process which exchanges $\tilde{u}_L$ makes the RH-quark-vector-current contribution

$$C'_{9,\mu} = -C'_{10,\mu} = -\frac{\sqrt{2}\pi^2}{G_F\eta_t e^2}\frac{\tilde{\lambda}'_{2i2}\tilde{\lambda}'^*_{2i3}}{m^2_{\tilde{u}_{Li}}}, \quad (3.1)$$

where the related operator $\mathcal{O}'_{9(10)}$ is given by P_L changed into P_R in $\mathcal{O}_{9(10)}$. This contribution is unwanted to explain $b \to s\ell^+\ell^-$ anomalies. Besides, the box diagrams of the $b \to s\ell^+\ell^-$ process also give such RH-quark-vector-current contributions which engage the sneutrino $\tilde{\nu}_{v^{(\prime)}}$ and LH slepton $\tilde{l}_{L\ell}$ with the coupling factors $\lambda'^{\mathcal{I}}_{vi2}\lambda'^{\mathcal{I}*}_{v'i3}$ and $\tilde{\lambda}'_{\ell i2}\tilde{\lambda}'^*_{\ell i3}$, respectively [see Eqs. (A2) and (A7)]. We concentrate on the loop effects of sneutrinos which are not expected to be heavily decoupled, and furthermore, the NP particles engaged in $b \to s\ell^+\ell^-$ and other related processes, such as $B \to X_s\gamma$, $B_s - \bar{B}_s$ mixing, etc., are expected to have masses at the sub-TeV or TeV scale, except for the heavy decoupled particles. Thus, we set the λ' couplings taken at the 0.5 TeV scale, called the $\mu_{\rm NP}$ scale, and assume λ'_{ijk} non-negligible with the single-value k at this scale. It is called the single-value k assumption in this work, and the index k is not to be summed over in equations from here on. This kind of assumption is also taken in recent works for the similar phenomenological consideration, such as in Refs. [43–47]. Authors of Ref. [45] further assume that $\lambda'_{ij1} = \lambda'_{ij2} = 0$, which are adopted in Refs. [46,47], considering the bounds of $\tau \to \mu\rho^0$ and $\tau \to \mu\phi$ decays, while these constraints can also be negligible by setting sufficiently heavy $m_{\tilde{u}_{Lj}}$.

We scrutinize all the one-loop Feynman diagrams of the $b \to s\ell^+\ell^-$ process in the RPV-MSSMIS under the single-value k assumption. For the box diagrams, there are eleven chargino box diagrams including nine λ' diagrams [Fig. 1(a)] and two non-λ' diagrams [Fig. 1(b)], fourteen W with W Goldstones or charged Higgs box (called $W/H^\pm$ box here) diagrams including ten λ' ones [Fig. 1(c)] and four non-λ' ones [Fig. 1(d)], and three $4\lambda'$ box diagrams [Figs. 1(e) and 1(f)]. The entire contributions of the box diagrams are listed in the Appendix (see formulas of the Passarino–Veltman functions D_2 and D_0 in Ref. [47], where $D_2(0)[m_1^2, m_2^2, m_3^2, m_4^2]$ is denoted as $D_2(0)[m_1, m_2, m_3, m_4]$ in this paper, respectively). The Wilson coefficients in the Appendix are given at $\mu_{\rm NP}$, and if we consider the single-value k assumption, only the LH-quark-vector-current contributions, $C^{\rm NP}_{9(10)}(\mu_{\rm NP})$, are existent and all the RH-quark-vector-current ones, $C'^{\rm NP}_{9(10)}(\mu_{\rm NP})$, vanish. Then the Wilson coefficients run down to the scale of $\mu_b = m_b$ under QCD renormalization. One can find that $C^{\rm NP}_{9(10)}(\mu_b) \approx C^{\rm NP}_{9(10)}(\mu_{\rm NP})$ [189] and $C'^{\rm NP}_{9(10)}(\mu_b)$ vanishes due to the approximate conservation of (axial-)vector currents. Thus we can

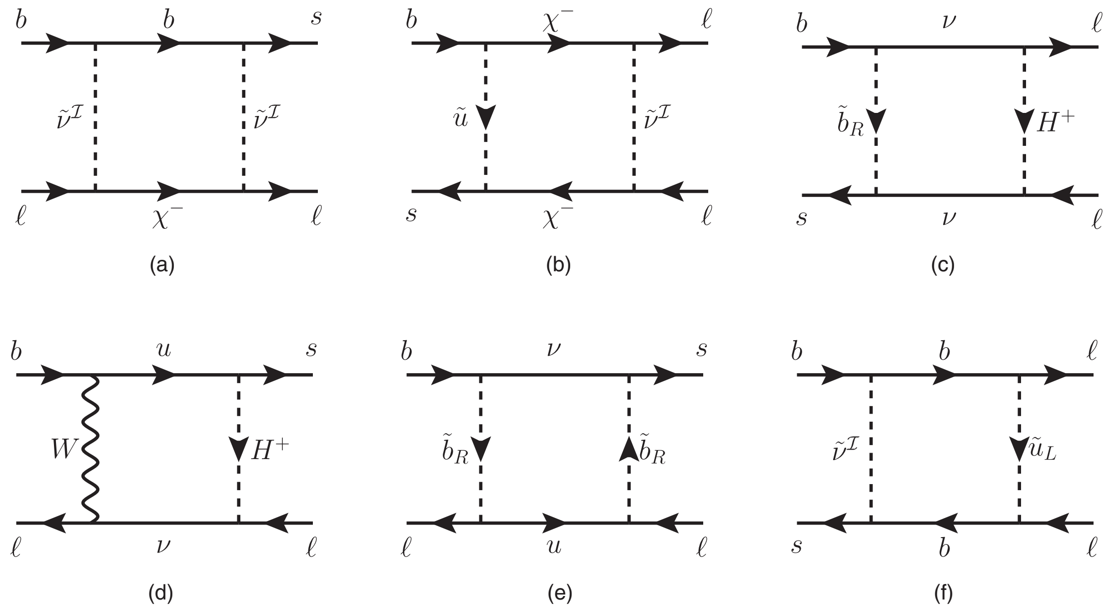

FIG. 1. Box diagrams for the $b \to s\ell^+\ell^-$ process in our parameter scheme. Figures 1(a) and 1(b) show an example of λ' diagrams and non-λ' diagrams within chargino boxes, respectively. Figures 1(c) and 1(d) show an example of λ' diagrams and non-λ' diagrams within the $W/H^{\pm}$ box, respectively. Figures 1(e) and 1(f) show the three $4\lambda'$ box diagrams with the $\tilde{\nu}^{\mathcal{R}}$-engaged diagram omitted.

constrain the model parameters related to $C_{9(10)}(\mu_b)$ using the global fit results introduced in Sec. I.

From the Appendix, one can see that $\tilde{l}_i$ and $\tilde{d}_{Lj}$ in the box diagrams can be forbidden under the assumption of a single-value k. In the following we further assume that $m_{\tilde{d}_{Rk}}$ is sufficiently heavy to focus on the contributions of sneutrinos as the bridge between the trilinear RPV term and the inverse seesaw mechanism. Therefore, contributions including $\tilde{d}_{Rk}$ are negligible and can be removed. Besides, we also set $m_{\tilde{u}_{Lj}}$ adequately heavy.[3] Because the LFU violating contributions, mainly from the $\mu^+\mu^-$ channel, are expected to explain $b \to s\ell^+\ell^-$ anomalies in both scenarios A and B, we will set that $\mathcal{M}^2_{\tilde{\nu}^{\mathcal{I}(R)}}$ has no flavor mixing and the electron-flavor elements with both LH and RH chirality are sufficiently heavy. Then nearly all box contributions to the $b \to se^+e^-$ transition, and some box contributions to the $b \to s\mu^+\mu^-$ transition, can be eliminated, and afterwards we show which contributions remain.

First among these non-negligible chargino box diagrams, the non-λ' diagram with RH sneutrinos previously discussed in Ref. [56] is recalculated by us. We find that the Wilson coefficient $C_9^{\rm NP}$ from this diagram equals to $-C_{10}^{\rm NP}$, which is different from the condition that $C_9^{\rm NP} = C_{10}^{\rm NP}$ in Ref. [56]. The related $C_9^{\rm NP}$, namely $C_{\rm V}^{\chi^{\pm}(1)}$ in this paper, is given by

$$C_{\rm V}^{\chi^{\pm}(1)} = -\frac{\sqrt{2}\pi^2 i}{2G_F\eta_t e^2} y_{u_i}^2 K_{i3}K_{i2}^* V_{m2}^* V_{n2}(g_2 V_{m1}\tilde{\mathcal{V}}_{v2}^{\mathcal{I}} - V_{m2}Y_{2v}^{\mathcal{I}})$$
$$(g_2 V_{n1}^* \tilde{\mathcal{V}}_{v2}^{\mathcal{I}} - V_{n2}^* Y_{2v}^{\mathcal{I}}) D_2[m_{\tilde{\nu}_v^{\mathcal{I}}}, m_{\chi_m^{\pm}}, m_{\chi_n^{\pm}}, m_{\tilde{u}_{Ri}}], \quad (3.2)$$

where the Yukawa couplings $y_{u_i} = \sqrt{2}m_{u_i}/v_u$ and $Y_{\ell v}^{\mathcal{I}} = (Y_\nu)_{j\ell}\tilde{\mathcal{V}}_{v(j+3)}^{\mathcal{I}*}$. This formula can be seen in the second term of Eq. (A1).

Then we show the λ' within the chargino box diagram containing the RPV interactions between singlet sneutrinos and quarks. The contribution is given by

$$C_{\rm V}^{\chi^{\pm}(2)} = \frac{\sqrt{2}\pi^2 i}{2G_F\eta_t e^2} \lambda_{v3k}'^{\mathcal{I}} \lambda_{v'2k}'^{\mathcal{I}*} (g_2 V_{m1}^* \tilde{\mathcal{V}}_{v2}^{\mathcal{I}} - V_{m2}^* Y_{2v}^{\mathcal{I}})$$
$$(g_2 V_{m1} \tilde{\mathcal{V}}_{v'2}^{\mathcal{I}} - V_{m2} Y_{2v'}^{\mathcal{I}}) D_2[m_{\tilde{\nu}_v^{\mathcal{I}}}, m_{\tilde{\nu}_{v'}^{\mathcal{I}}}, m_{\chi_m^{\pm}}, m_{d_k}], \quad (3.3)$$

which appears in the third term of Eq. (A1).

The nonignorable $W/H^{\pm}$ box contributions in Eq. (A3) are

$$C_{9,\ell}^{W/H^{\pm}(1)} = -C_{10,\ell}^{W/H^{\pm}(1)} = -\frac{\sqrt{2}\pi^2 i}{2G_F\eta_t e^2} (y_{u_i}^2 K_{i3}K_{i2}^* Z_{H_{h2}}^2 Z_{H_{h'2}}^2 |Y_{\ell v}^{\mathcal{N}}|^2 D_2[m_{\nu_v}, m_{u_i}, m_{H_h}, m_{H_{h'}}]$$
$$-4g_2^2 m_{u_i} y_{u_i} m_{\nu_v} K_{i3}K_{i2}^* Z_{H_{h2}}^2 {\rm Re}(\mathcal{V}_{v\ell} Y_{\ell v}^{\mathcal{N}*}) D_0[m_{\nu_v}, m_{u_i}, m_W, m_{H_h}] + 5g_2^4 K_{i3}K_{i2}^* |\mathcal{V}_{v\ell}|^2 D_2[m_{\nu_v}, m_{u_i}, m_W, m_W]), \quad (3.4)$$

[3]In this work, $m_{\tilde{d}_{Rk}}$ and $m_{\tilde{u}_{Lj}}$ are set to be around 10 TeV.

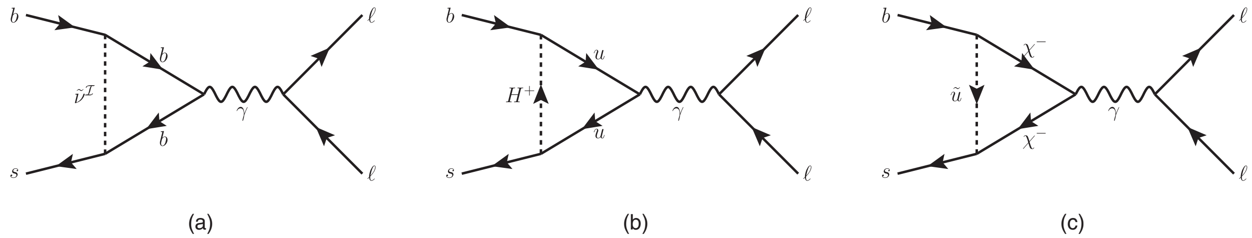

FIG. 2. Photon penguin diagrams for the $b \to s\ell^+\ell^-$ process in our parameter scheme. Here each example of the λ' diagrams (left), the non-λ' diagrams with $W/H^\pm$ (middle), and charginos (right) engaged are shown respectively.

where the mixing matrix elements $Z_{H_{12}} = -\sin\beta$ and $Z_{H_{22}} = -\cos\beta$, with Goldstone mass $m_{H_1} = m_W$ and charged Higgs mass $m_{H_2} = m_{H^\pm}$, and $Y^{\mathcal{N}}_{\ell v} = (Y_\nu)_{j\ell}\mathcal{V}^*_{v(j+3)}$. It is obvious that these $W/H^\pm$ box contributions include SM effects, which cannot be separated naively from NP effects because of the generation and the chiral mixing of massive neutrinos. In addition, these contributions still contain both the $\mu^+\mu^-$ channel sector and e^+e^- channel sector. We will further investigate these contributions in detail in Sec. V.

Next we show the penguin contributions. Indeed, the Wilson coefficients of Z-boson penguin diagrams are negligible. While the contributions of photon penguin diagrams can be nonignorable, where the λ' diagrams [Fig. 2(a)] give

$$C_{\mathrm{U}}^{\gamma(1)} = -\frac{\sqrt{2}\lambda'^{\mathcal{I}}_{v33}\lambda'^{\mathcal{I}*}_{v23}}{36G_F\eta_t m^2_{\tilde{\nu}^{\mathcal{I}}_v}}\left(\frac{4}{3} + \log\frac{m_b^2}{m^2_{\tilde{\nu}^{\mathcal{I}}_v}}\right) \tag{3.5}$$

for the case of $k = 3$, and the non-λ' contributions [Figs. 2(b) and 2(c)], namely $C_{\mathrm{U}}^{\gamma(2)}$, are also calculated by us for completeness.

IV. THE $(g-2)_\ell$ AND OTHER CONSTRAINTS

In this section, we introduce the NP contributions to $(g-2)_\ell$ and other related processes.

A. The muon (electron) anomalous magnetic moment

The amplitude of the $\ell \to \ell\gamma$ ($\ell = e, \mu$) transition is given by

$$i\mathcal{M} = ie\bar{\ell}\left(\gamma^\eta + a_\ell \frac{i\sigma^{\eta\beta}q_\beta}{2m_\ell}\right)\ell A_\eta \tag{4.1}$$

in the zero limit of photon moment q. The second term in the bracket gives the loop corrections and a_ℓ is called the anomalous magnetic moment for the related lepton.

The SM-like diagrams that only involve SM particles give the same contributions to a_ℓ as the SM. Hence the SUSY part can contribute to the observed anomaly Δa_ℓ [141]. The one-loop chargino and neutralino contributions in the RPV-MSSMIS are given here, with reference to Refs. [122,128,141,190], as

$$\begin{aligned}
\delta a_\ell^{\chi^\pm} &= \frac{m_\ell}{16\pi^2}\left[\frac{m_\ell}{6m^2_{\tilde{\nu}_v}}(|c^{\ell L}_{mv}|^2 + |c^{\ell R}_{mv}|^2)F_1^C(m^2_{\chi^\pm_m}/m^2_{\tilde{\nu}_v}) \right.\\
&\quad \left. + \frac{m_{\chi^\pm_m}}{m^2_{\tilde{\nu}_v}}\mathrm{Re}(c^{\ell L}_{mv}c^{\ell R}_{mv})F_2^C(m^2_{\chi^\pm_m}/m^2_{\tilde{\nu}_v})\right],\\
\delta a_\ell^{\chi^0} &= \frac{m_\ell}{16\pi^2}\left[-\frac{m_\ell}{6m^2_{\tilde{l}_i}}(|n^{\ell L}_{ni}|^2 + |n^{\ell R}_{ni}|^2)F_1^N(m^2_{\chi^0_n}/m^2_{\tilde{l}_i}) \right.\\
&\quad \left. + \frac{m_{\chi^0_n}}{m^2_{\tilde{l}_i}}\mathrm{Re}(n^{\ell L}_{ni}n^{\ell R}_{ni})F_2^N(m^2_{\chi^0_n}/m^2_{\tilde{l}_i})\right],
\end{aligned} \tag{4.2}$$

where

$$\begin{aligned}
c^{\ell R}_{mv} &= y_\ell U_{m2}\tilde{\mathcal{V}}^{\mathcal{I}}_{v\ell}, \qquad c^{\ell L}_{mv} = -g_2 V_{m1}\tilde{\mathcal{V}}^{\mathcal{I}}_{v\ell} + V_{m2}Y^{\mathcal{I}}_{\ell v},\\
n^{\ell R}_{ni} &= \sqrt{2}g_1 N_{n1}\delta_{i(\ell+3)} + y_\ell N_{n3}\delta_{i\ell},\\
n^{\ell L}_{ni} &= \frac{1}{\sqrt{2}}(g_2 N_{n2} + g_1 N_{n1})\delta_{i\ell} - y_\ell N_{n3}\delta_{i(\ell+3)},
\end{aligned} \tag{4.3}$$

and with functions

$$\begin{aligned}
F_1^C(x) &= \frac{1}{(1-x)^4}(2 + 3x - 6x^2 + x^3 + 6x\log x),\\
F_2^C(x) &= -\frac{1}{(1-x)^3}(3 - 4x + x^2 + 2\log x),\\
F_1^N(x) &= \frac{1}{(1-x)^4}(1 - 6x + 3x^2 + 2x^3 - 6x^2\log x),\\
F_2^N(x) &= \frac{1}{(1-x)^3}(1 - x^2 + 2x\log x).
\end{aligned} \tag{4.4}$$

The flavor mixing of RH sleptons is not considered here, and neither is the flavor mixing of LH sleptons. Since the contributions from λ' diagrams are negligible for the heavy $\tilde{b}_R$ and $\tilde{u}_L$, they are not shown in Eq. (4.3). The difference from the MSSM is the form factor $c^{\ell L}_{mv}$ in Eq. (4.3), where the extra $V_{m2}Y^{\mathcal{I}}_{\ell v}$ term can make an enhancement. Because the measured Δa_e has different features when compared with Δa_μ, we consider the schemes of $|\delta a_\mu^{\chi^\pm}| \gg |\delta a_e^{\chi^\pm}| \approx 0$ and $|\delta a_e^{\chi^0}| \gg |\delta a_\mu^{\chi^0}| \approx 0$ [131]. Thus, the muon generation associated with RH sleptons is set sufficiently heavy, as well as heavy $\tilde{L}'_1$ which is already assumed in Sec. III. Afterwards we expect $1.92(1.33) \leqslant |\delta a_\mu^{\chi^\pm} + \delta a_\mu^{\chi^0}| \times 10^9 \leqslant 3.10(3.69)$ to be in accord with a_μ data at $1(2)\sigma$, respectively.

B. Tree-level processes

In the following we investigate related transition bounds which exchange $\tilde{d}_{Rk}$ at the tree level. On account of the assumption of heavy $m_{\tilde{d}_{Rk}} \sim 10$ TeV, the neutral current processes $B \to K^{(*)}\nu\bar{\nu}$, $B \to \pi\nu\bar{\nu}$, and $D^0 \to \mu^+\mu^-$, as well as the charged current processes $B \to \tau\nu$, $D_s \to \tau\nu$, and $\tau \to K\nu$, provide no effective constraints. Besides, there are some tree-level processes which may make some slight bounds to mention here.

The SM prediction $\mathcal{B}(K^+ \to \pi^+\nu\bar{\nu})_{\rm SM} = (9.24 \pm 0.83) \times 10^{-11}$ [191], combined with the experimental measurement $\mathcal{B}(K^+ \to \pi^+\nu\bar{\nu})_{\rm exp} = (1.7 \pm 1.1) \times 10^{-10}$ [192], induces the constraint. The effective Lagrangian for the $K \to \pi\nu\bar{\nu}$ decay can be described by

$$\mathcal{L}_{\rm eff} = (C^{\rm SM}\delta_{ii'} + C^{\rm NP}_{ii'})(\bar{d}\gamma_\mu P_L s)(\bar{\nu}_i\gamma^\mu P_L \nu_{i'}) + {\rm H.c.}, \quad (4.5)$$

where the SM contributes $C^{\rm SM} = -\frac{\sqrt{2}G_F e^2 K_{ts}K^*_{td}}{4\pi^2 \sin^2\theta_W} X(x_t)$ and $X(x_t) = \frac{x_t(x_t+2)}{8(x_t-1)} + \frac{3x_t(x_t-2)}{8(x_t-1)^2}\log(x_t)$ with $x_t = m_t^2/m_W^2$ [193], while the NP contribution is

$$C^{\rm NP}_{ii'} = \frac{\lambda'^{\mathcal{N}}_{i'2k}\lambda'^{\mathcal{N}*}_{i1k}}{2m^2_{\tilde{d}_{Rk}}}. \quad (4.6)$$

Then the bound is obtained as $|\lambda'^{\mathcal{N}}_{i'2k}\lambda'^{\mathcal{N}*}_{i1k}| < 0.074$ when $m_{\tilde{d}_{Rk}}$ is around 10 TeV [47], and, hence, we can set $|\lambda'_{i1k}| \lesssim 10^{-2}$ to avoid this bound.

As to the processes of τ decaying to a μ and a vector meson, $\tau \to \mu\rho^0$ and $\tau \to \mu\phi$, the branching fraction is given by [194]

$$\mathcal{B}(\tau \to \mu V) = \frac{\tau_\tau f_V^2 m_\tau^3}{128\pi}|A_V|^2\left(1 - \frac{m_V^2}{m_\tau^2}\right)\left(1 + \frac{m_V^2}{m_\tau^2} - 2\frac{m_V^4}{m_\tau^4}\right), \quad (4.7)$$

where V stands for ρ^0 and ϕ. The mean lifetime of the tauon $\tau_\tau = 290.3 \pm 0.5$ fs [192], and the decay constants f_V have the value of $f_{\rho^0} = 153$ MeV and $f_\phi = 237$ MeV, respectively [45]. A_V is given by [194]

$$A_{\rho^0} = \frac{\tilde{\lambda}'_{3j1}\tilde{\lambda}'^*_{2j1}}{2m^2_{\tilde{u}_{Lj}}} - \frac{\tilde{\lambda}'_{31k}\tilde{\lambda}'^*_{21k}}{2m^2_{\tilde{d}_{Rk}}},$$
$$A_\phi = \frac{\tilde{\lambda}'_{3j2}\tilde{\lambda}'^*_{2j2}}{2m^2_{\tilde{u}_{Lj}}}. \quad (4.8)$$

The most recent experimental upper limits on the branch fractions of the two processes at 90% confidence level (C.L.) are $\mathcal{B}(\tau \to \mu\rho^0) < 1.2 \times 10^{-8}$ and $\mathcal{B}(\tau \to \mu\phi) < 8.4 \times 10^{-8}$ [192]. We can obtain the bounds [45]

$$|\tilde{\lambda}'_{3j1}\tilde{\lambda}'^*_{2j1} - \tilde{\lambda}'_{31k}\tilde{\lambda}'^*_{21k}| < 1.9, \qquad |\tilde{\lambda}'_{3j2}\tilde{\lambda}'^*_{2j2}| < 3.6 \quad (4.9)$$

when both $m_{\tilde{d}_{Rk}}$ and $m_{\tilde{u}_{Lj}}$ are around 10 TeV. Under the negligible $|\lambda'_{i1k}|$ assumption, the bounds of Eq. (4.9) turn into $|\tilde{\lambda}'_{321}\tilde{\lambda}'^*_{221} + \tilde{\lambda}'_{331}\tilde{\lambda}'^*_{231}| < 1.9$ or $|\tilde{\lambda}'_{322}\tilde{\lambda}'^*_{222} + \tilde{\lambda}'_{332}\tilde{\lambda}'^*_{232}| < 3.6$ when the single-value k is restricted to 1 or 2 for the nonzero λ'_{ijk}, respectively, while there exists no effective bound when k is restricted to 3. We can see that if k is restricted to 1(2) for the nonzero λ'_{ijk}, $|\lambda'_{ij1(2)}|$ should be below around 1(1.3), respectively, in the case of no cancelling out.

C. $B \to X_s\gamma$

At the one-loop level, the photon penguin diagrams in Fig. 2 also contribute to the electromagnetic dipole operator $\mathcal{O}_7 = \frac{m_b}{e}(\bar{s}\sigma^{\mu\nu}P_R b)F_{\mu\nu}$ constrained by the $B \to X_s\gamma$ decay. The NP Wilson coefficient $C_7^{\rm NP}$ includes charged Higgs contributions and the effects from the chargino with $\tilde{u}_{Rj}$ as well as the RPV contributions engaging sneutrinos.

The RPV contribution is given by

$$C_7^{\rm RPV} = \frac{\sqrt{2}\lambda'^{\mathcal{I}}_{v3k}\lambda'^{\mathcal{I}*}_{v2k}}{144G_F\eta_t m^2_{\tilde{\nu}^{\mathcal{I}}_v}}. \quad (4.10)$$

Compared with $C_{\rm U}^{\gamma(1)}$ in Eq. (3.5), $C_7^{\rm RPV}$ contains the common part $\lambda'^{\mathcal{I}}_{v3k}\lambda'^{\mathcal{I}*}_{v2k}/m^2_{\tilde{\nu}^{\mathcal{I}}_v}$ while containing no logarithmic term.

The charged Higgs contribution is given by

$$C_7^{H^\pm} = \frac{1}{3\tan^2\beta}F_7^{(1)}(y_t) + F_7^{(2)}(y_t), \quad (4.11)$$

where the form factors are $F_7^{(1)}(y_t) = \frac{y_t(7-5y_t-8y_t^2)}{24(y_t-1)^3} + \frac{y_t^2(3y_t-2)}{4(y_t-1)^4}\log y_t$ and $F_7^{(2)}(y_t) = \frac{y_t(3-5y_t)}{12(y_t-1)^2} + \frac{y_t(3y_t-2)}{6(y_t-1)^3}\log y_t$, with $y_t = m_t^2/m^2_{H^\pm}$. One can see that the $F_7^{(2)}(y_t)$ part is not suppressed when $\tan\beta$ is large, and this is unlike the $H^\pm$ contributions to $C_{9(10)}$ which are entirely suppressed by the large $\tan\beta$. The formulas of $C_7^{\chi^\pm}$ engaging the chargino, together with $\tilde{u}_{Rj}$ and the QCD corrections, can be seen in Ref. [195].

The recent measurements of the branching ratio $\mathcal{B}(B \to X_s\gamma)_{\rm exp} \times 10^4 = 3.43 \pm 0.21 \pm 0.07$ [89] is consistent with the SM prediction $\mathcal{B}(B \to X_s\gamma)_{\rm SM} \times 10^4 = 3.36 \pm 0.23$ [196], and induces the bound to $|C_7^{\rm NP}| < 0.025$ [48].

D. $B_s - \bar{B}_s$ mixing

Another process we should consider is $B_s - \bar{B}_s$ mixing, mastered by the Lagrangian

$$\mathcal{L}_{\rm eff} = (C^{\rm SM}_{B_s} + C^{\rm NP}_{B_s})(\bar{s}\gamma_\mu P_L b)(\bar{s}\gamma^\mu P_L b) + {\rm H.c.}, \tag{4.12}$$

where the non-negligible NP contribution is given by

$$\begin{aligned} C^{\rm NP}_{B_s} = -\frac{i}{8}(&\lambda'^{\mathcal{I}}_{v3k}\lambda'^{\mathcal{I}*}_{v2k}\lambda'^{\mathcal{I}}_{v'3k}\lambda'^{\mathcal{I}*}_{v'2k}D_2[m_{\tilde{\nu}^{\mathcal{I}}_v}, m_{\tilde{\nu}^{\mathcal{I}}_{v'}}, m_{d_k}, m_{d_k}] \\ &+ y^2_{u_i}y^2_{u_j}(K_{i3}K^*_{i2})(K_{j3}K^*_{j2})|V_{m2}V_{n2}|^2 \\ &\times D_2[m_{\chi^\pm_m}, m_{\chi^\pm_n}, m_{\tilde{u}_{Ri}}, m_{\tilde{u}_{Rj}}]), \end{aligned} \tag{4.13}$$

including the λ' diagram with double sneutrinos and the non-λ' diagram with double RH su-quarks, and the SM contribution $C^{\rm SM}_{B_s} = -\frac{1}{4\pi^2}G_F^2 m_W^2 \eta_t^2 S(x_t)$ with the function $S(x_t) = \frac{x_t(4-11x_t+x_t^2)}{4(x_t-1)^2} + \frac{3x_t^3\log(x_t)}{2(x_t-1)^3}$. With the measurement of $\Delta M_s^{\rm exp} = (17.757 \pm 0.021)\ {\rm ps}^{-1}$ [89],[4] the recent SM prediction $\Delta M_s^{\rm SM} = (18.4^{+0.7}_{-1.2})\ {\rm ps}^{-1} = (1.04^{+0.04}_{-0.07})\Delta M_s^{\rm exp}$ [198] leads to the bound of

$$0.90 < |1 + C^{\rm NP}_{B_s}/C^{\rm SM}_{B_s}| < 1.11, \tag{4.14}$$

at the 2σ level.

E. Lepton flavor violating decays

We discuss the lepton flavor violating decays including $\tau \to \ell\gamma$, $\mu \to e\gamma$, $\tau \to \ell\ell\ell$, $\mu \to eee$, and $\tau \to \ell'\ell\ell$. First, the λ'-diagram contributions can be eliminated when $\tilde{b}_R$ is sufficiently heavy [47]. As to the non-λ' diagrams, all the neutralino-slepton diagrams contain flavor mixings of charged sleptons and all the chargino-sneutrino diagrams contain flavor mixings of sneutrinos (see Ref. [199] for concrete formulas). So, the effects of these two kinds of diagrams vanish when there is no flavor mixing in the two mass matrices. For contributions of the $W/H^\pm$-neutrino diagrams, they are always connected to these terms, which are $\mathcal{V}^{T*}_{(\alpha+3)v}\mathcal{V}^{T}_{(\beta+3)v}$, $\mathcal{V}^{T*}_{(\alpha+3)v}\mathcal{V}^{T}_{\beta v}$, and $\mathcal{V}^{T*}_{\alpha v}\mathcal{V}^{T}_{\beta v}$, and their conjugate terms, where $\alpha, \beta = e, \mu, \tau$ and $\alpha \neq \beta$ [199]. In Sec. VA, we will show how all these terms contribute no effects under the particular structure of the neutrino mass matrix. The same analyses can also be applied to the non-λ' diagrams in $B_s^0 \to \tau^\pm\mu^\mp$ and $B^+ \to K^+\tau^\pm\mu^\mp$. For the λ' diagrams of these two processes, we refer to the detailed discussions in Ref. [46], and no obvious constraints are found.

F. Anomalous $t \to cV(h)$ decays

The SM predicts the branching ratios of $t \to cV$ decays (V stands for the vector bosons, including Z, γ, and the gluon g) and $t \to ch$ decay (h stands for SM-like Higgs boson) below the scale of 10^{-15}–10^{-12} [200] due to the Glashow–Iliopoulos–Maiani suppression. This scale is beyond the detection capabilities at the collider in the near future. The most recent experimental 95% C.L. upper limits on the branching ratios of these top quark decays at the Large Hadron Collider (LHC) show that $\mathcal{B}(t \to cZ) < 2.4 \times 10^{-4}$ [201], $\mathcal{B}(t \to c\gamma) < 1.8 \times 10^{-4}$ [202], $\mathcal{B}(t \to cg) < 4.1 \times 10^{-4}$ [203], and $\mathcal{B}(t \to ch) < 1.1 \times 10^{-3}$ [204]. Compared with the effects from pure MSSM, the one-loop RPV diagrams can make more contributions [205,206], and hence we will investigate these effects in our model.

For the $t \to cV$ decays, the effective tcV vertices are expressed as

$$\begin{aligned} V^\mu(tcZ) &= ie(\gamma^\mu P_L A^Z + ik_\nu\sigma^{\mu\nu}P_R B^Z), \\ V^\mu(tc\gamma) &= ie(ik_\nu\sigma^{\mu\nu}P_R B^\gamma), \\ V^\mu(tcg) &= ig_s t^a(ik_\nu\sigma^{\mu\nu}P_R B^g), \end{aligned} \tag{4.15}$$

where k_ν is the momentum of the vector boson. The form factors A^Z and B^V are given by [205]

$$\begin{aligned} A^Z &= \frac{\tilde{\lambda}'^*_{i2k}\tilde{\lambda}'_{i3k}}{16\pi^2}\left\{f_1^Z B_1(m_t, m_{d_k}, m_{\tilde{l}_{Li}}) - f_2^Z\left[2c_{24} - \frac{1}{2} + m_Z^2(c_{12}+c_{23})\right](-p_t, p_c, m_{d_k}, m_{\tilde{l}_{Li}}, m_{d_k})\right. \\ &\quad \left. - f_3^Z[2c_{24} + m_t^2(c_{11} - c_{12} + c_{21} - c_{23})](-p_t, k, m_{d_k}, m_{\tilde{l}_{Li}}, m_{\tilde{l}_{Li}})\right\}, \\ B^V &= \frac{\tilde{\lambda}'^*_{i2k}\tilde{\lambda}'_{i3k}}{16\pi^2}\{f_2^V m_t[c_{11} - c_{12} + c_{21} - c_{23}](-p_t, p_c, m_{d_k}, m_{\tilde{l}_{Li}}, m_{d_k}) \\ &\quad - f_3^V m_t[c_{11} - c_{12} + c_{21} - c_{23}](-p_t, k, m_{d_k}, m_{\tilde{l}_{Li}}, m_{\tilde{l}_{Li}})\}, \end{aligned} \tag{4.16}$$

[4]The newly updated experimental result of ΔM_s by LHCb has been reported [197]. The combined result with previous LHCb measurements gives $\Delta M_s^{\rm LHCb} = (17.7656 \pm 0.0057)\ {\rm ps}^{-1}$ with the improved precision. Using this new combined result will not change Eq. (4.14).

where p_t and p_c are the momentums of top and charm quarks and functions B_1 and c_{ij} are the Passarino–Veltman integrals totally referring to Ref. [207]. The constants $f_1^Z = \frac{3-4\sin^2\theta_W}{6\sin\theta_W\cos\theta_W}$, $f_2^Z = -\frac{\sin\theta_W}{3\cos\theta_W}$, and $f_3^Z = \frac{2\sin^2\theta_W - 1}{\sin\theta_W\cos\theta_W}$ are in the form factors A^Z and B^Z. In B^γ, the relevant constants are $f_2^\gamma = 1/3$ and $f_3^\gamma = -1$, while $f_2^g = -1$ and $f_3^g = 0$ in B^g. Then the decay widths of $t \to cV$ are given as

$$\begin{aligned}\Gamma(t \to cZ)_{\mathrm{NP}} &= \frac{e^2(m_t^2 - m_Z^2)^2}{32\pi m_t^3}\left[\left(2 + \frac{m_t^2}{m_Z^2}\right)|A^Z|^2\right.\\ &\quad\left. - 6m_t \mathrm{Re}(A^Z B^{Z*}) + (2m_t^2 + m_Z^2)|B^Z|^2\right],\\ \Gamma(t \to c\gamma)_{\mathrm{NP}} &= \frac{e^2 m_t^3}{16\pi}|B^\gamma|^2,\\ \Gamma(t \to cg)_{\mathrm{NP}} &= \frac{g_s^2 m_t^3}{12\pi}|B^g|^2. \end{aligned} \tag{4.17}$$

As for the $t \to ch$ decay, the effective tch vertex is expressed as

$$V(tch) = ie(P_L A_L^h + P_R A_R^h). \tag{4.18}$$

After omitting masses of charm quarks and all down-type quarks, one can obtain [206]

$$\begin{aligned} A_R^h &= \frac{\tilde{\lambda}'^*_{i2k}\tilde{\lambda}'_{i3k}}{16\pi^2}\mathcal{Y}_{\tilde{l}_{Li}} m_t (c_{11} - c_{12})(-p_t, k, 0, m_{\tilde{l}_{Li}}, m_{\tilde{l}_{Li}}),\\ A_L^h &= 0, \end{aligned} \tag{4.19}$$

where factor $\mathcal{Y}_{\tilde{l}_{Li}} \approx \frac{m_Z}{\sin\theta_W\cos\theta_W}(\frac{1}{2} - \sin^2\theta_W)\cos 2\beta$ when the masses of leptons are omitted and the mass of CP-odd Higgs bosons is sufficiently heavy. Then the decay width of $t \to ch$ is

$$\Gamma(t \to ch)_{\mathrm{NP}} = \frac{e^2(m_t^2 - m_h^2)^2}{32\pi m_t^3}|A_R^h|^2. \tag{4.20}$$

NP contributes to related branching ratios which are given by $\mathcal{B}(t \to cV(h))_{\mathrm{NP}} = \Gamma(t \to cV(h))_{\mathrm{NP}}/\Gamma(t \to bW)_{\mathrm{SM}}$, where the dominant decay $t \to bW$ has the SM prediction $\Gamma(t \to bW)_{\mathrm{SM}} = 1.42$ GeV [208].

G. LHC direct searches

The LHC direct searches have led to stringent limits on the masses of sbottoms and stops [209–215], and the recent searches [213–215] have excluded the heavy stops more than 1.35 TeV. In view of the fact that $\tilde{d}_{Rk}$ and $\tilde{u}_{Li}$ have already been set adequately heavy, we further set $m_{\tilde{u}_{Ri}} > 1.4$ TeV.

For the constraints on LH sleptons as mentioned in Sec. II, when considering nonzero λ couplings, the lower bounds of $m_{\tilde{\nu}_L}$ and $m_{\tilde{l}}$ reach the TeV scale [182–184]. Because only nonzero λ' couplings are restricted in this work, LH sleptons decaying to pure leptons directly is secondary, and processes without λ interactions should be taken into consideration mainly. We consider the searches which focus on LH sleptons decaying into leptons and the lightest neutralino χ_1^0 [216–218], and the recent ATLAS results [217] show that the LH sleptons that are heavier than χ_1^0 can avoid the exclusion for $m_{\chi_1^0} \gtrsim 300$ GeV. Besides, the compressed scenario, that the lightest chargino mass $m_{\chi_1^\pm}$ is slightly heavier than $m_{\chi_1^0}$ [219], is adopted. Thus we will let inputs induce $m_{\chi_1^\pm} \gtrsim m_{\chi_1^0} \gtrsim 300$ GeV and $m_{\tilde{l}_L} > 300$ GeV.

V. NUMERICAL RESULTS AND DISCUSSIONS

In this section, we investigate $b \to s\ell^+\ell^-$ anomalies numerically, as well as the a_μ anomaly and the related constraints.

A. Choice of input parameters

The first parts of the input parameters used throughout the paper are collected in Table I, which includes the lepton oscillation data [74] under the normal ordering (NO) assumption of LH neutrino masses. In addition, we further keep $\delta_{\mathrm{CP}} = \pi$ to omit the CP violation in U^{PMNS}. The lightest neutrino mass is set to zero to have the masses of three-flavor light neutrinos as $\{0, 0.008, 0.05\}$ eV with $m_\nu^{\mathrm{diag}} \approx \mathrm{diag}(0, \sqrt{\Delta m_{21}^2}, \sqrt{\Delta m_{31}^2})$ [220]. Then we collect the fixed values of relevant model parameters in Table II. The sets give $m_{\chi_1^\pm} = 325$ GeV and $m_{\chi_1^0} = 307$ GeV, which are in accordance with the constraints discussed in Sec. IV G. Besides, we set the diagonal parameters for Y_ν, M_R, $m_{\tilde{L}'}$, $m_{\tilde{R}}$, B_{M_R}, and A_ν in Eq. (2.7) so that the sneutrino mixing matrices $\tilde{\mathcal{V}}^{\mathcal{I}(R)}$ only have chiral mixings without flavor mixings and let them have proper values to agree with the discussions in Secs. III and IV.[5] As for the remaining model parameters, $m_{\tilde{L}_2'}$, $m_{\tilde{L}_3'}$, λ'_{22k}, λ'_{23k}, λ'_{32k}, and λ'_{33k}, they can vary freely in the ranges considered.

With related inputs in Tables I and II, the μ_S term in Eq. (2.4) can be figured out with m_D, M_R, U^{PMNS}, and the light neutrino masses m_ν^{diag} through Eq. (2.5). Then we obtain the approximate numerical form of the mixing matrix $\mathcal{V}^T$,

[5]Under the premise of no flavor mixing in $\tilde{\mathcal{V}}^{\mathcal{I}(R)}$, we mention that sufficiently heavy $m_{\tilde{L}_1'}$ and $m_{\tilde{R}_1}$ can eliminate the box contributions to $b \to se^+e^-$ except for $C_{9,e}^{W/H^\pm(1)}$ in Sec. III; $m_{\tilde{\mu}_R}$ and $m_{\tilde{L}_1'}$ are set sufficiently heavy for the scheme of nondominant $|\delta a_\mu^{\chi^0}|$ and $|\delta a_e^{\chi^\pm}|$ in Sec. IV A. The $\tilde{\mathcal{V}}^{\mathcal{I}(R)}$ without flavor mixings is also for satisfying the bounds from lepton flavor violating decays mentioned in Sec. IV E.

TABLE I. Summary of parts of input parameters used throughout this paper.

QCD and EW parameters [192]					
$G_F[10^{-5}\ \mathrm{GeV}^{-2}]$	$\alpha_e(m_Z)$	$\alpha_s(m_Z)$	m_W [GeV]	$\sin^2\theta_W$	
1.1663787	1/128	0.1179(10)	80.379	0.2312	
Quark and lepton masses [GeV] [192]					
$\bar{m}_b(\bar{m}_b)$	$\bar{m}_c(\bar{m}_c)$	m_t	m_e	m_μ	m_τ
$4.18^{+0.03}_{-0.02}$	1.27(2)	172.76(30)	0.511×10^{-3}	0.1057	1.777
CKM Wolfenstein parameters [221]					
λ_{CKM}	A	$\bar{\rho}$	$\bar{\eta}$		
$0.22484^{+0.00025}_{-0.00006}$	$0.8235^{+0.0056}_{-0.0145}$	$0.1569^{+0.0102}_{-0.0061}$	$0.3499^{+0.0079}_{-0.0065}$		
Lepton oscillation parameters (NO) [74]					
$\sin^2\theta_{12}$	$\sin^2\theta_{23}$	$\sin^2\theta_{13}$			
0.304(12)	$0.573^{+0.016}_{-0.020}$	$0.02219^{+0.00062}_{-0.00063}$			
$\delta_{CP}[°]$	$\Delta m^2_{21}[10^{-5}\ \mathrm{eV}^2]$	$\Delta m^2_{31}[10^{-3}\ \mathrm{eV}^2]$			
197^{+27}_{-24}	$7.42^{+0.21}_{-0.20}$	$2.517^{+0.026}_{-0.028}$			

$$\mathcal{V}^T \approx \begin{pmatrix} 0.840 & 0.509 & -0.147 & -0.085i & 0 & 0 & 0.085 & 0 & 0 \\ -0.231 & 0.599 & 0.755 & 0 & 0.097i & 0 & 0 & 0.097 & 0 \\ 0.478 & -0.608 & 0.628 & 0 & 0 & 0.061i & 0 & 0 & -0.061 \\ 0 & 0 & 0 & 0.707i & 0 & 0 & 0.707 & 0 & 0 \\ 0 & 0 & 0 & 0 & -0.707i & 0 & 0 & 0.707 & 0 \\ 0 & 0 & 0 & 0 & 0 & -0.707i & 0 & 0 & -0.707 \\ -0.102 & -0.062 & 0.018 & -0.702i & 0 & 0 & 0.702 & 0 & 0 \\ 0.032 & -0.083 & -0.105 & 0 & 0.700i & 0 & 0 & 0.700 & 0 \\ -0.041 & 0.053 & -0.055 & 0 & 0 & 0.704i & 0 & 0 & -0.704 \end{pmatrix}, \tag{5.1}$$

corresponding to the light neutrino masses $m_{\nu_i} = \{0, 0.008, 0.05\}$ eV and the nearly degenerate heavy ones $m_{\nu_{v_h}}$ around 1 TeV. One can see that there is no flavor mixing when the RH sector is engaged but chiral mixing exists. With the numerical result of Eq. (5.1), we can eliminate the $\mathcal{V}^{T*}_{(\alpha+3)v}\mathcal{V}^T_{(\beta+3)v}$ and $\mathcal{V}^{T*}_{(\alpha+3)v}\mathcal{V}^T_{\beta v}$ terms in the contributions of $W/H^\pm$-neutrino diagrams to the lepton flavor violating decays within Sec. IV E. $\mathcal{V}^{T*}_{\alpha v}\mathcal{V}^T_{\beta v}$ can be decomposed into the following two parts: $\sum_{v_h=4}^9 \mathcal{V}^{T*}_{\alpha v_h}\mathcal{V}^T_{\beta v_h}$ and $\sum_{i=1}^3 \mathcal{V}^{T*}_{\alpha i}\mathcal{V}^T_{\beta i} = -\sum_{v_h=4}^9 \mathcal{V}^{T*}_{\alpha v_h}\mathcal{V}^T_{\beta v_h}$, related to the nearly degenerate heavy neutrinos and light neutrinos, respectively [188]. It can also be found that $\mathcal{V}^{T*}_{\alpha v}\mathcal{V}^T_{\beta v}$ provides no effects from Eq. (5.1). In sum, the lepton flavor violating decays mentioned in Sec. IV E contribute no effective bounds in our input sets.

TABLE II. The sets of fixed model parameters, defined at μ_{NP} scale. The two sets of A_ν are for scenario A and B, respectively.

Parameters	Sets	Parameters	Sets
$\tan\beta$	15	Y_ν	diag(0.7,0.8,0.5) [222]
M_1	320 GeV	M_R	diag(1,1,1) TeV
M_2	350 GeV	B_{M_R}	diag(0.5, 0.5, 0.5) TeV^2
μ	450 GeV	A_ν	0; diag(0, −1.5, 0) TeV
$m_{\tilde{u}_{Ri}}$	1.5 TeV	$m_{\tilde{L}'_1}$	5 TeV
$m_{\tilde{\mu}_R}$	5 TeV	$m_{\tilde{R}}$	diag(5,0,0) TeV

In the following we discuss the feature of $C^{W/H^\pm(1)}_{9(10),\ell}$ in Eq. (3.4), which includes the e^+e^- channel. The three terms of Eq. (3.4) contain $|\mathcal{V}^T_{(\ell+3)v}|^2$, $\mathrm{Re}(\mathcal{V}^T_{\ell v}\mathcal{V}^T_{(\ell+3)v})$ and $|\mathcal{V}^T_{\ell v}|^2$, respectively. For h or/and $h'=2$ first, this part of Eq. (3.4) includes the contribution of charged Higgs bosons and it can be ignored for the set of $\tan\beta = 15$. In the case of $h = h' = 1$, this part of Eq. (3.4) describes the contribution of seesaw-extended SM. $|\mathcal{V}^T_{\ell v}|^2$ in the third term is dominated by $|U^{\mathrm{PMNS}}_{\ell i}|^2$, and thus this term is nearly equal to the contribution of the original SM. Because $\mathrm{Re}(\mathcal{V}^T_{\ell v}\mathcal{V}^T_{(\ell+3)v})$ is negligible compared with $|\mathcal{V}^T_{(\ell+3)v}|^2$, we focus on the first term in Eq. (3.4) and the second term can be omitted safely. According to the discussion above, the pure NP contribution $\Delta C^{W/H^\pm}_{9(10),\ell}$ in Eq. (3.4) is induced by only heavy neutrinos and is given by

$$\Delta C_{9,\ell}^{W/H^\pm} = \sum_{v_h=4}^{9} -\frac{\sqrt{2}\pi^2 i}{2G_F\eta_t e^2} y_{u_i}^2 K_{i3} K_{i2}^* \sin^4\beta |Y_{\nu_{\ell\ell}} \mathcal{V}_{(\ell+3)v_h}^T|^2 \times D_2[m_{\nu_{v_h}}, m_{u_i}, m_W, m_W]. \quad (5.2)$$

Our parameter set leads that the contribution $\Delta C_{9,\ell}^{W/H^\pm} = -\Delta C_{10,\ell}^{W/H^\pm}$ in Eq. (5.2) is at a negative 10^{-2} scale for both $\mu^+\mu^-$ and e^+e^- channels. This small LFU effect cannot be included in both $C_{\rm V}$ and $C_{\rm U}$ within Eq. (1.3) and is ignored for the approximation. We also obtain $C_{\rm U}^{\gamma(2)}$ around 0.01 and $C_{\rm V}^{\chi^\pm(1)}$ around −0.01 in which the main contributions are from λ' diagrams. In summary, the LFU violating coefficient and the LFU coefficient can be represented by $C_{\rm V} = C_{\rm V}^{\chi^\pm(1)} + C_{\rm V}^{\chi^\pm(2)}$ and $C_{\rm U} = C_{\rm U}^{\gamma(1)} + C_{\rm U}^{\gamma(2)}$, respectively. We find that the factor $c_{mv}^{\mu L} = -g_2 V_{m1} \tilde{\mathcal{V}}_{v2}^{\mathcal{I}} + V_{m2} Y_{2v}^{\mathcal{I}}$ in Eq. (4.3) is also included in $C_{\rm V}^{\chi^\pm(1)}$ and $C_{\rm V}^{\chi^\pm(2)}$. Therefore, the large chiral mixing of sneutrinos will make some enhancements to both $C_{\rm V}$ and $a_\mu^{\rm NP}$ simultaneously.

B. Explanations of $b \to s\ell^+\ell^-$ anomalies with $(g-2)_\mu$

In this part we will search for the common areas of five variables, $m_{\tilde{L}_2'}$, λ'_{223}, λ'_{233}, λ'_{323}, and λ'_{333}, to explain $b \to s\ell^+\ell^-$ anomalies as well as $(g-2)_\mu$ deviations considering related constraints in the two fit scenarios mentioned in Sec. I. In scenario A, we fix $m_{\tilde{L}_3'} = m_{\tilde{L}_2'} - 50$ GeV which is a benefit for satisfying the constraint of $B_s - \bar{B}_s$ mixing. In scenario B, we fix $m_{\tilde{L}_3'} = m_{\tilde{L}_2'}$. For the bounds of $m_{\tilde{l}_L}$ in LHC searches mentioned in Sec. IV G, we focus on $m_{\tilde{L}_2'} \geq 370$ GeV which causes the mass of lightest charged slepton $m_{\tilde{l}_1}$ (sneutrino $m_{\tilde{\nu}_1}$) to be above 318(301) GeV in scenario A and $m_{\tilde{\nu}_1}$ to be heavier than 100 GeV, while $m_{\tilde{l}_1}$ is above 352 GeV in scenario B. In particular, we choose $k = 3$ for a benchmark of the numerical calculation.

1. Explanations of $(g-2)_\mu$ anomalies

At first, we show the bound for $m_{\tilde{L}_2'}$ with $a_\mu^{\rm NP}$ in each scenario at Fig. 3, in which $a_\mu^{\rm NP}$ can contribute to $a_\mu^{\rm SM}$ increasing and accommodate the observed Δa_μ deviation from the 4.2σ to 2σ level below. In scenario B, there are also allowed spaces at the 1σ level. In scenario A, we obtain the allowed range $370 \leq m_{\tilde{L}_2'} \leq 470$ GeV at the 2σ level, and in scenario B there is a larger range of $370 \leq m_{\tilde{L}_2'} \leq 820$ GeV at the 2σ level as well as a range of $420 \leq m_{\tilde{L}_2'} \leq 610$ GeV at the 1σ level. Besides, we have calculated that $a_e^{\rm NP}$ can reach negative $\mathcal{O}(10^{-14})$ only in the case of $m_{\tilde{e}_R} \sim 100$ GeV in our parameter spaces.

2. Results in scenario A

Next we investigate $b \to s\ell^+\ell^-$ anomalies further with the parameter regions of $m_{\tilde{L}_2'}$ we have obtained above. In scenario A, $C_{\rm U}$ should have 0 as the definition. To make $C_{\rm U}$ cancel out, $\lambda'^*_{323}\lambda'_{333}$ is figured out as the expression of $\lambda'^*_{223}\lambda'_{223}$ and vice versa, and the constraints from $B_s - \bar{B}_s$ mixing and $B \to X_s\gamma$ will be mainly suppressed. Also the large $m_{H^\pm}$ as 2 TeV and $m_{\tilde{u}_{Ri}}$ as 1.5 TeV avoid too strong of bounds on the MSSM part of the model from $B \to X_s\gamma$ decays. In Fig. 4, the common areas of $b \to s\ell^+\ell^-$ explanations under other bounds show a larger value and region of $\lambda'^*_{223}\lambda'_{233}$ or $-\lambda'^*_{323}\lambda'_{333}$ for a heavier $m_{\tilde{L}_2'}$. The values of $\lambda'^*_{323}\lambda'_{333}$ always have the negative sign compared with the positive $\lambda'^*_{223}\lambda'_{233}$, and their region sizes are nearly the same

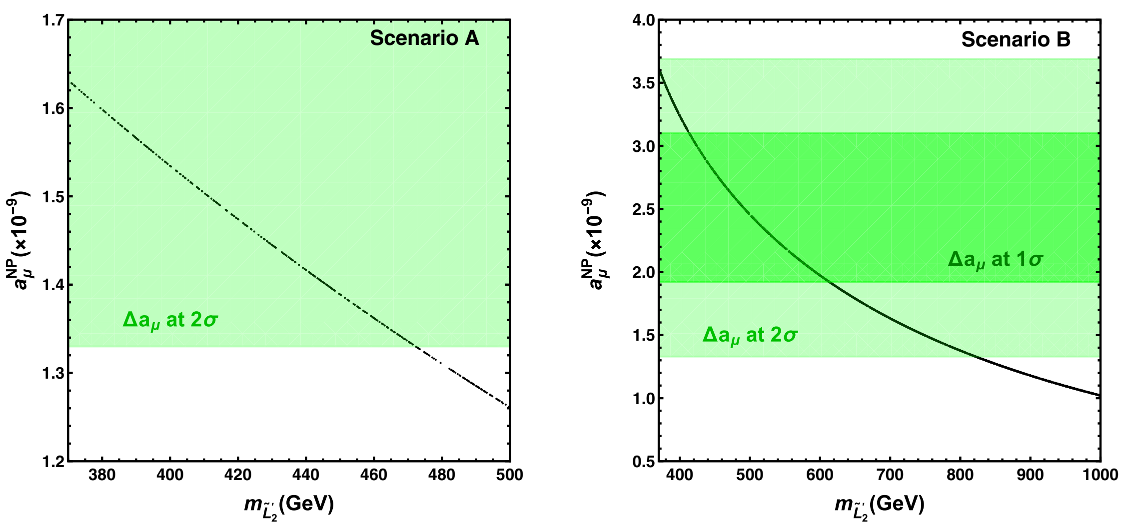

FIG. 3. $a_\mu^{\rm NP}$ varies with $m_{\tilde{L}_2'}$ in scenario A (left) and scenario B (right). The dark (light) green areas are 1(2)σ favored to explain the Δa_μ deviation.

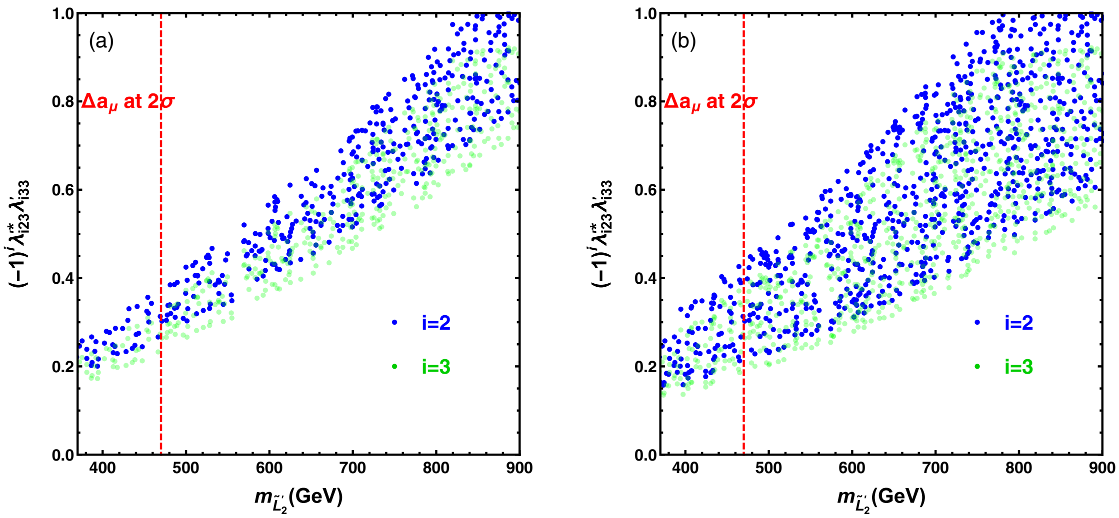

FIG. 4. The common scopes of constraints with the fit level of rare B-meson decays as 1σ (left) and 2σ (right) in scenario A. The blue (green) points show that $\lambda'^*_{223}\lambda'_{233}$ ($-\lambda'^*_{323}\lambda'_{333}$) varies with $m_{\tilde{L}_2'}$ and then $\lambda'^*_{323}\lambda'_{333}$ ($\lambda'^*_{223}\lambda'_{233}$) is derived. It should be paid attention to that among $\lambda'^*_{223}\lambda'_{233}$ and $\lambda'^*_{323}\lambda'_{333}$ there is only one independent variable in this scenario, so the blue and green points are relevant. The area on the left of the red dashed line is allowed to be accordant with a_μ data at 2σ.

for the same value of $m_{\tilde{L}_2'}$. The results in scenario A show that $b \to s\ell^+\ell^-$ anomalies in both 1σ and 2σ fits can be explained.

Combined with considering the Δa_μ deviation, we find the final common region to explain the $b \to s\ell^+\ell^-$ and a_μ anomalies simultaneously at the 2σ level, which are shown by the points on the left of the Δa_μ bound line in Fig. 4(b). The result provides the $m_{\tilde{L}_2'}$ range with 370 GeV $\leq m_{\tilde{L}_2'} \leq$ 470 GeV and the edge values of λ' combinations are collected in Table III.

3. Results in scenario B

In scenario B, the common scopes are shown at Figs. 5 and 6. Similar to scenario A, the values of allowed $\lambda'^*_{323}\lambda'_{333}$ are always negative compared with the positive $\lambda'^*_{223}\lambda'_{233}$ and the region sizes of their common scopes become larger as $m_{\tilde{L}_2'}$ is varying heavier. As shown in Fig. 5, there exist areas to explain $b \to s\ell^+\ell^-$ anomalies at the 1σ level for rare B-meson decay fits, and the $B_s - \bar{B}_s$ mixing mostly constrains. While $B \to X_s\gamma$ decays provide no extra bounds when $m_{\tilde{L}_2'} \gtrsim 430$ GeV and even reaches TeV. When $m_{\tilde{L}_2'}$ blow around 430 GeV, 1σ explanations will not be viable, and $B \to X_s\gamma$ decays provide extra bounds versus $B_s - \bar{B}_s$ mixing. In Fig. 6(a), we compare the common region sizes for the different fixed $m_{\tilde{L}_2'}$ with each other and find that the deviation between the allowed region sizes of $\lambda'^*_{223}\lambda'_{233}$ and $-\lambda'^*_{323}\lambda'_{333}$ are small, up to around 0.1 scale. Thus we further fix them equaling each other and show $\lambda'^*_{223}\lambda'_{233}$ varying with increasing $m_{\tilde{L}_2'}$ only in Fig. 6(b), and find that the 1σ favored fit requires $m_{\tilde{L}_2'} \gtrsim 550$ GeV and the region of 2σ fit has a broader size. When $m_{\tilde{L}_2'}$ is below 550 GeV, there also exists common regions of 1σ fit while in these regions, $\lambda'^*_{223}\lambda'_{233} + \lambda'^*_{323}\lambda'_{333} \neq 0$.

Combined with a_μ data, the final common region of 400 GeV $\leq m_{\tilde{L}_2'} \leq$ 820 GeV is required to explain the $b \to s\ell^+\ell^-$ and a_μ anomalies simultaneously at the 2σ level, and edge values of λ' combinations are collected in Table IV.

TABLE III. The edge values of $\lambda'^*_{223}\lambda'_{233}$ and $\lambda'^*_{323}\lambda'_{333}$ related to different $m_{\tilde{L}_2'}$ for the simultaneous explanation of $b \to s\ell^+\ell^-$ and a_μ anomalies at the 2σ level in scenario A.

$m_{\tilde{L}_2'}$ [GeV]	$\lambda'^*_{223}\lambda'_{233}$	$\lambda'^*_{323}\lambda'_{333}$
370	[0.14, 0.30]	[−0.26, −0.12]
420	[0.17, 0.37]	[−0.32, −0.15]
470	[0.20, 0.44]	[−0.38, −0.18]

C. Predictions of $t \to cg$ decay

As in the numerical discussions above, we have the final parameter spaces of $m_{\tilde{L}_2'}$, as well as the coupling combinations $\lambda'^*_{223}\lambda'_{233}$ and $\lambda'^*_{323}\lambda'_{333}$, to explain related LFU violating anomalies, while these variables also provide NP effects on the top decays $t \to cV(h)$.

We have checked that our final parameter spaces can satisfy the most recent upper limits on the branching ratios of $t \to cV(h)$ decays at the LHC easily. The NP contributions to the branching ratios of $t \to cV(h)$ depend on the term $\tilde{\lambda}'^*_{i2k}\tilde{\lambda}'_{i3k}f_{\tilde{l}_{Li}}$ where $f_{\tilde{l}_{Li}}$ stands for the loop integral including LH charged sleptons. This term can be given

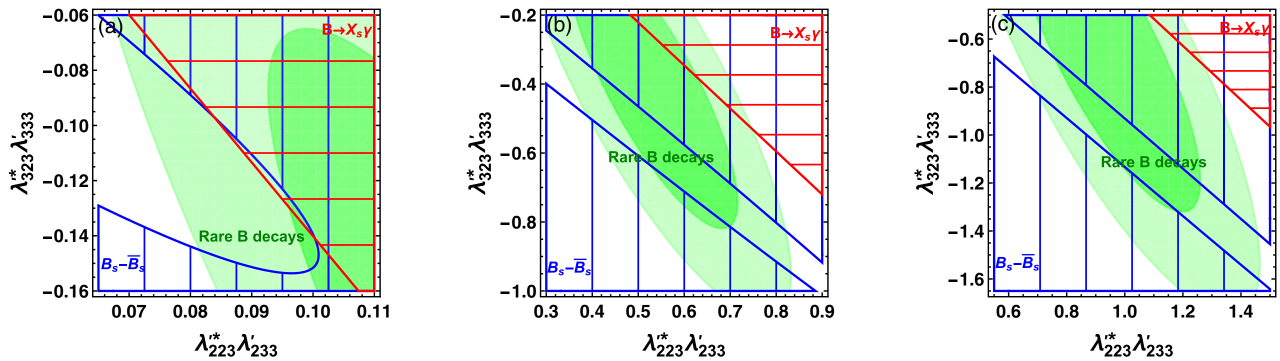

FIG. 5. The regions of constraints in scenario B without a_μ data. The green regions are $1(2)\sigma$ favored ones with dark (light) opacity to satisfy the rare B-meson decay fits. At the 2σ level, the hatched blue areas are excluded by $B_s - \bar{B}_s$ mixing and the hatched red areas are excluded by $B \to X_s\gamma$ decays. Besides, $m_{\tilde{L}'_3} = m_{\tilde{L}'_2}$ are fixed as 430 (left), 750 (middle), and 1000 GeV (right).

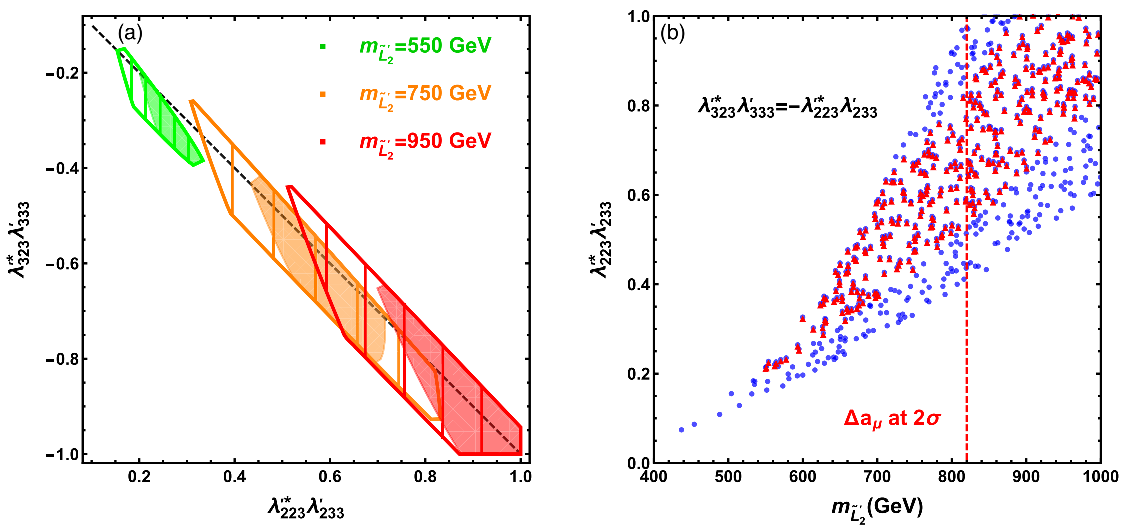

FIG. 6. The common scopes of constraints in scenario B. Figure 6(a) shows the common scopes constrained by the rare B-meson decay fits at the 1σ level denoted by painted areas and the 2σ level denoted by hatched areas, combined with other process constraints at the 2σ level for $m_{\tilde{L}'_3} = m_{\tilde{L}'_2} = 550$ (green), 750 (orange), and 950 GeV (red). Figure 6(b) shows the regions which satisfy the rare B-meson decay fits being $1(2)\sigma$ favored under the assumption $\lambda'^{*}_{323}\lambda'_{333} = -\lambda'^{*}_{223}\lambda'_{233}$, denoted by red (blue) points, with other process constraints being considered. The area on the left of the red dashed line is allowed to be accordant with a_μ data at 2σ.

by $\tilde{\lambda}'^{*}_{i2k}\tilde{\lambda}'_{i3k} f_{\tilde{l}_{Li}} \approx (\lambda'^{*}_{i2k}\lambda'_{i3k} + |\lambda'_{i2k}|^2 K_{cb} + |\lambda'_{i3k}|^2 K_{cb}) f_{\tilde{l}_{Li}}$. Because of canceling out in $\lambda'^{*}_{i2k}\lambda'_{i3k} f_{\tilde{l}_{Li}}$, the hierarchical structure between λ'_{a2k} and λ'_{a3k} $(a = 2, 3)$ is considered to make prominent contributions, and we set the large λ'_{a3k} here. We keep restricting k as 3 and set $\lambda'_{233} = \lambda'_{333} = 2$ or 3.

TABLE IV. The same as Table III except for scenario B.

$m_{\tilde{L}'_2}$ [GeV]	$\lambda'^{*}_{223}\lambda'_{233}$	$\lambda'^{*}_{323}\lambda'_{333}$
420	[0.062, 0.086]	[−0.137, −0.063]
650	[0.22, 0.62]	[−0.70, −0.17]
820	[0.35, 1.00]	[−1.10, −0.30]

In the following we show that the prediction values of $\mathcal{B}(t \to cg)_{\rm NP}$ from the parameter spaces to explain $b \to s\ell^+\ell^-$ and a_μ anomalies can reach the sensitivity at the FCC-hh in Fig. 7. One can see that in scenario A, when $370\ \text{GeV} \le m_{\tilde{L}'_2} \le 440$ GeV and $\lambda'_{a33} = 3$, the prediction $\mathcal{B}(t \to cg)_{\rm NP}$ is higher than the prospective upper limit 9.87×10^{-8}, at the 100 TeV FCC-hh for the integrated luminosity of $\mathcal{L} = 10\ \text{ab}^{-1}$ of data through the triple-top signal [223], and the prediction in scenario B for the same λ'_{a33} can also reach this upper limit. When λ'_{a33} is set to be 2, the branching ratio is much lower and can not even reach

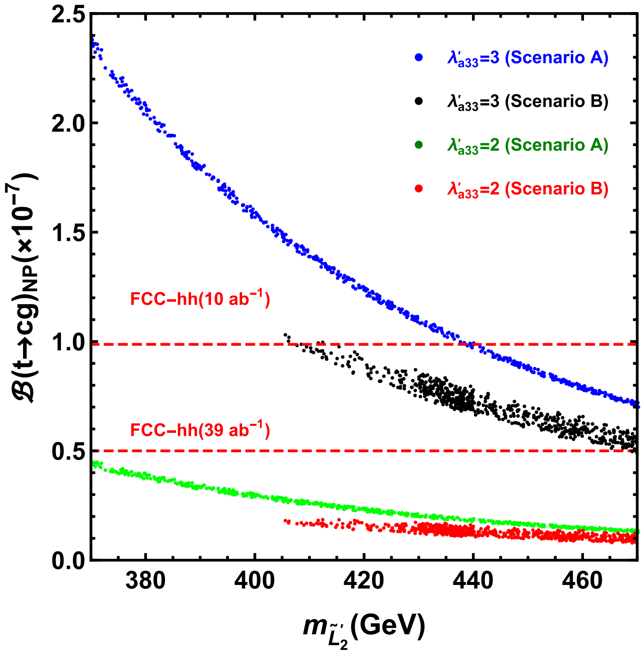

FIG. 7. The predictions of $\mathcal{B}(t \to cg)_{\rm NP}$ compared with the prospect upper limit at the 100 TeV FCC-hh.

the sensitivity at the FCC-hh for the estimated $\mathcal{L} = 39\ \mathrm{ab}^{-1}$ in both scenarios A and B. We conclude that, at the FCC-hh, this model signal on the $t \to cg$ transition has considerable possibilities to be found for sufficiently large λ'_{a33}, but the model can escape easily from the bound of this transition when the structure between λ'_{a23} and λ'_{a33} is not hierarchical enough.

VI. CONCLUSIONS

Recent measurements on the transition $b \to s\ell^+\ell^-$ reveal the deviations from SM predictions. The most motivative $R_K^{(*)}$ anomaly and anomalies from other observables like P'_5, called $b \to s\ell^+\ell^-$ anomalies collectively, suggest the NP of LFU violation may exist. Besides, these NP may also affect the enduring muon anomalous magnetic moment, the $(g-2)_\mu$ problem.

In this work, we have studied the chiral mixing effects of sneutrinos in the R-parity violating MSSM with the inverse seesaw mechanism to explore the explanation of $b \to s\ell^+\ell^-$ anomalies with the $(g-2)_\mu$ problem simultaneously. Here all the one-loop contributions to $b \to s\ell^+\ell^-$ processes are scrutinized under the assumption of a single-value k. Among them, the contributions of chiral mixing between LH and singlet (s)neutrinos within a superpotential term $\lambda'_{ijk}\hat{L}_i\hat{Q}_j\hat{D}_k$ are given for the first time to our knowledge. To explain $b \to s\ell^+\ell^-$ anomalies in this model, two kinds of model-independent global fits are adopted. One is the single-parameter scenario of $C^{\rm NP}_{9,\mu} = -C^{\rm NP}_{10,\mu}$ and the other scenario is the double-parameter one in which $(\pm)C_{\rm V}$ contributes to the $C^{\rm NP}_{9(10),\mu}$ part in the $\mu^+\mu^-$ channel and $C_{\rm U}$ contributes to the $C^{\rm NP}_9$ part in both the $\mu^+\mu^-$ and e^+e^- channels. Then in the numerical analyses, we find that $b \to s\ell^+\ell^-$ and $(g-2)_\mu$ anomalies can be explained simultaneously in both scenario A and B. The main constraints among related processes are from $B_s - \bar{B}_s$ mixing covering $B \to X_s\gamma$ decay mostly, but the other tree-level and one-loop processes provide no effective bounds. At last, we make a prospect that NP contributions to $t \to cg$ process can reach the sensitivity at the FCC-hh in parts of the parameter spaces of this model.

ACKNOWLEDGMENTS

We thank Yi-Lei Tang, Chengfeng Cai, and Seishi Enomoto for valuable discussions. This work is supported in part by the National Natural Science Foundation of China under Grant No. 11875327, the Fundamental Research Funds for the Central Universities, and the Sun Yat-Sen University Science Foundation.

APPENDIX: ONE-LOOP BOX CONTRIBUTIONS IN THE RPV-MSSMIS

In this Appendix, we list all Wilson coefficients from the one-loop box diagrams of $b \to s\ell^+\ell^-$ in the RPV-MSSMIS without the extra assumption of a single-value k.

The LH-quark-current contributions of chargino box diagrams to the $b \to s\ell^+\ell^-$ process are given by

$$\begin{aligned}
C^{\chi^\pm}_{9,\ell} = -C^{\chi^\pm}_{10,\ell} = -\frac{\sqrt{2}\pi^2 i}{2G_F\eta_t e^2}\Big(& g_2^2 K_{i3}K^*_{i2}V^*_{m1}V_{n1}(g_2V_{m1}\tilde{\mathcal{V}}^{\mathcal{I}}_{v\ell}-V_{m2}Y^{\mathcal{I}}_{\ell v})(g_2V^*_{n1}\tilde{\mathcal{V}}^{\mathcal{I}}_{v\ell}-V^*_{n2}Y^{\mathcal{I}}_{\ell v})D_2[m_{\tilde{\nu}^{\mathcal{I}}_v},m_{\chi^\pm_m},m_{\chi^\pm_n},m_{\tilde{u}_{Li}}]\\
&+y^2_{u_i}K_{i3}K^*_{i2}V^*_{m2}V_{n2}(g_2V_{m1}\tilde{\mathcal{V}}^{\mathcal{I}}_{v\ell}-V_{m2}Y^{\mathcal{I}}_{\ell v})(g_2V^*_{n1}\tilde{\mathcal{V}}^{\mathcal{I}}_{v\ell}-V^*_{n2}Y^{\mathcal{I}}_{\ell v})D_2[m_{\tilde{\nu}^{\mathcal{I}}_v},m_{\chi^\pm_m},m_{\chi^\pm_n},m_{\tilde{u}_{Ri}}]\\
&-\lambda'^{\mathcal{I}}_{v3k}\lambda'^{\mathcal{I}*}_{v'2k}(g_2V^*_{m1}\tilde{\mathcal{V}}^{\mathcal{I}}_{v\ell}-V^*_{m2}Y^{\mathcal{I}}_{\ell v})(g_2V_{m1}\tilde{\mathcal{V}}^{\mathcal{I}}_{v'\ell}-V_{m2}Y^{\mathcal{I}}_{\ell v'})D_2[m_{\tilde{\nu}^{\mathcal{I}}_v},m_{\tilde{\nu}^{\mathcal{I}}_{v'}},m_{\chi^\pm_m},m_{d_k}]\\
&-\tilde{\lambda}'_{\ell ik}\tilde{\lambda}'^*_{\ell jk}g_2^2K_{i3}K^*_{j2}|V_{m1}|^2D_2[m_{\tilde{u}_{Li}},m_{\tilde{u}_{Lj}},m_{\chi^\pm_m},m_{d_k}]+\tilde{\lambda}'_{\ell ik}\lambda'^{\mathcal{I}*}_{v2k}(g_2K_{i3}V^*_{m1})(g_2V_{m1}\tilde{\mathcal{V}}^{\mathcal{I}}_{v\ell}-V_{m2}Y^{\mathcal{I}}_{\ell v})D_2[m_{\tilde{\nu}^{\mathcal{I}}_v},m_{\tilde{u}_{Li}},m_{\chi^\pm_m},m_{d_k}]\\
&+\lambda'^*_{\ell ik}\lambda'^{\mathcal{I}}_{v3k}(g_2K^*_{i2}V_{m1})(g_2V^*_{m1}\tilde{\mathcal{V}}^{\mathcal{I}}_{v\ell}-V^*_{m2}Y^{\mathcal{I}}_{\ell v})D_2[m_{\tilde{\nu}^{\mathcal{I}}_v},m_{\tilde{u}_{Li}},m_{\chi^\pm_m},m_{d_k}]\Big),
\end{aligned} \tag{A1}$$

where the Yukawa couplings are $y_{u_i} = \sqrt{2}m_{u_i}/v_u$ and $Y^{\mathcal{I}}_{\ell v} = (Y_\nu)_{j\ell}\tilde{\mathcal{V}}^{\mathcal{I}*}_{v(j+3)}$, while the corresponding RH-quark-current contributions are

$$C'^{\chi^\pm}_{9,\ell} = -C'^{\chi^\pm}_{10,\ell} = -\frac{\sqrt{2}\pi^2 i}{2G_F\eta_t e^2}\lambda'^{\mathcal{I}}_{vi2}\lambda'^{\mathcal{I}*}_{v'i3}(g_2V^*_{m1}\tilde{\mathcal{V}}^{\mathcal{I}}_{v\ell} - V^*_{m2}Y^{\mathcal{I}}_{\ell v})(g_2V_{m1}\tilde{\mathcal{V}}^{\mathcal{I}}_{v'\ell} - V_{m2}Y^{\mathcal{I}}_{\ell v'})D_2[m_{\tilde{\nu}^{\mathcal{I}}_v}, m_{\tilde{\nu}^{\mathcal{I}}_{v'}}, m_{\chi^\pm_m}, m_{d_i}]. \quad \text{(A2)}$$

The contributions of $W/H^\pm$ box diagrams to the $b \to s\ell^+\ell^-$ process are given by

$$\begin{aligned}
C^{W/H^\pm}_{9,\ell} = -C^{W/H^\pm}_{10,\ell} = -\frac{\sqrt{2}\pi^2 i}{2G_F\eta_t e^2}\big(&y^2_{u_i}K_{i3}K^*_{i2}Z^2_{H_{h2}}Z^2_{H_{h'2}}|Y^{\mathcal{N}}_{\ell v}|^2 D_2[m_{\nu_v}, m_{u_i}, m_{H_h}, m_{H_{h'}}] \\
&- 4g_2^2 m_{u_i}y_{u_i}m_{\nu_v}K_{i3}K^*_{i2}Z^2_{H_{h2}}\mathrm{Re}(\mathcal{V}_{v\ell}Y^{\mathcal{N}*}_{\ell v})D_0[m_{\nu_v}, m_{u_i}, m_W, m_{H_h}] \\
&+ 5g_2^4 K_{i3}K^*_{i2}|\mathcal{V}_{v\ell}|^2 D_2[m_{\nu_v}, m_{u_i}, m_W, m_W] \\
&+ Z^2_{H_{h2}}Y^{\mathcal{N}*}_{\ell v}Y^{\mathcal{N}}_{\ell v'}\lambda'^{\mathcal{N}}_{v3k}\lambda'^{\mathcal{N}*}_{v'3k}D_2[m_{\nu_v}, m_{\nu_{v'}}, m_{H_h}, m_{\tilde{d}_{Rk}}] \\
&- 2g_2^2 m_{\nu_v}m_{\nu_{v'}}\mathcal{V}^*_{v\ell}\mathcal{V}_{v'\ell}\lambda'^{\mathcal{N}}_{v3k}\lambda'^{\mathcal{N}*}_{v'2k}D_0[m_{\nu_v}, m_{\nu_{v'}}, m_W, m_{\tilde{d}_{Rk}}] \\
&+ 2m_{\nu_v}m_{\nu_{v'}}Z^2_{H_{h2}}Y^{\mathcal{N}}_{\ell v}Y^{\mathcal{N}*}_{\ell v'}\lambda'^{\mathcal{N}}_{v3k}\lambda'^{\mathcal{N}*}_{v'2k}D_0[m_{\nu_v}, m_{\nu_{v'}}, m_{H_h}, m_{\tilde{d}_{Rk}}] \\
&+ 2m_{u_i}m_{u_j}y_{u_i}y_{u_j}K_{i3}K^*_{j2}Z^2_{H_{h2}}\tilde{\lambda}'_{\ell ik}\tilde{\lambda}'^*_{\ell jk}D_0[m_{u_i}, m_{u_j}, m_{H_h}, m_{\tilde{d}_{Rk}}] \\
&- g_2^2\mathcal{V}_{v\ell}\mathcal{V}^*_{v'\ell}\lambda'^{\mathcal{N}}_{v3k}\lambda'^{\mathcal{N}*}_{v'2k}D_2[m_{\nu_v}, m_{\nu_{v'}}, m_W, m_{\tilde{d}_{Rk}}] \\
&- g_2^2 K_{i3}K^*_{j2}\tilde{\lambda}'_{\ell ik}\tilde{\lambda}'^*_{\ell jk}D_2[m_{u_i}, m_{u_j}, m_W, m_{\tilde{d}_{Rk}}] \\
&- 2m_{u_i}y_{u_i}m_{\nu_v}K_{i3}Z^2_{H_{h2}}Y^{\mathcal{N}*}_{\ell v}\tilde{\lambda}'_{\ell ik}\lambda'^{\mathcal{N}*}_{v'2k}D_0[m_{u_i}, m_{\nu_v}, m_{H_h}, m_{\tilde{d}_{Rk}}] \\
&- 2m_{u_i}y_{u_i}m_{\nu_v}K^*_{i2}Z^2_{H_{h2}}Y^{\mathcal{N}}_{\ell v}\tilde{\lambda}'^*_{\ell ik}\lambda'^{\mathcal{N}}_{v3k}D_0[m_{u_i}, m_{\nu_v}, m_{H_h}, m_{\tilde{d}_{Rk}}] \\
&+ g_2^2 K^*_{i2}\mathcal{V}_{v\ell}\tilde{\lambda}'^*_{\ell ik}\lambda'^{\mathcal{N}}_{v3k}D_2[m_{u_i}, m_{\nu_v}, m_W, m_{\tilde{d}_{Rk}}] \\
&+ g_2^2 K_{i3}\mathcal{V}^*_{v\ell}\tilde{\lambda}'_{\ell ik}\lambda'^{\mathcal{N}*}_{v2k}D_2[m_{u_i}, m_{\nu_v}, m_W, m_{\tilde{d}_{Rk}}]\big),
\end{aligned} \quad \text{(A3)}$$

$$\begin{aligned}
C'^{W/H^\pm}_{9,\ell} = -C'^{W/H^\pm}_{10,\ell} = -\frac{\sqrt{2}\pi^2 i}{2G_F\eta_t e^2}\big(&-2Z^2_{H_{h2}}Y^{\mathcal{N}*}_{\ell v}Y^{\mathcal{N}}_{\ell v'}\lambda'^{\mathcal{N}}_{v'i2}\lambda'^{\mathcal{N}*}_{vi3}m_{\nu_v}m_{\nu_{v'}}D_0[m_{\nu_v}, m_{\nu_{v'}}, m_{H_h}, m_{\tilde{d}_{Li}}] \\
&- Z^2_{H_{h2}}Y^{\mathcal{N}}_{\ell v}Y^{\mathcal{N}*}_{\ell v'}\lambda'^{\mathcal{N}}_{v'i2}\lambda'^{\mathcal{N}*}_{vi3}D_2[m_{\nu_v}, m_{\nu_{v'}}, m_{H_h}, m_{\tilde{d}_{Li}}] \\
&+ g_2^2\mathcal{V}_{v\ell}\mathcal{V}^*_{v'\ell}\lambda'^{\mathcal{N}}_{vi2}\lambda'^{\mathcal{N}*}_{v'i3}D_2[m_{\nu_v}, m_{\nu_{v'}}, m_W, m_{\tilde{d}_{Li}}] \\
&+ 2g_2^2\mathcal{V}_{v\ell}\mathcal{V}^*_{v'\ell}\lambda'^{\mathcal{N}}_{v'i2}\lambda'^{\mathcal{N}*}_{vi3}m_{\nu_v}m_{\nu_{v'}}D_0[m_{\nu_v}, m_{\nu_{v'}}, m_W, m_{\tilde{d}_{Li}}]\big),
\end{aligned} \quad \text{(A4)}$$

where the mixing matrix elements are $Z_{H_{12}} = -\sin\beta$, $Z_{H_{22}} = -\cos\beta$, with the Goldstone mass $m_{H_1} = m_W$ and charged Higgs mass $m_{H_2} = m_{H^\pm}$ and $Y^{\mathcal{N}}_{\ell v} = (Y_\nu)_{j\ell}\mathcal{V}^*_{v(j+3)}$.

The contributions of $4\lambda'$ box diagrams to the $b \to s\ell^+\ell^-$ process are given by

$$\begin{aligned}
C^{4\lambda'}_{9,\ell} = -C^{4\lambda'}_{10,\ell} = -\frac{\sqrt{2}\pi^2 i}{2G_F\eta_t e^2}\big(&\tilde{\lambda}'_{\ell ik}\tilde{\lambda}'^*_{\ell ik'}\lambda'^{\mathcal{N}}_{v3k'}\lambda'^{\mathcal{N}*}_{v2k}D_2[m_{\nu_v}, m_{u_i}, m_{\tilde{d}_{Rk}}, m_{\tilde{d}_{Rk'}}] \\
&+ \tilde{\lambda}'_{\ell ik'}\tilde{\lambda}'^*_{\ell ik}\lambda'^{\mathcal{I}}_{v3k}\lambda'^{\mathcal{I}*}_{v2k'}D_2[m_{\tilde{\nu}^{\mathcal{I}}_v}, m_{\tilde{u}_{Li}}, m_{d_k}, m_{d_{k'}}]\big),
\end{aligned} \quad \text{(A5)}$$

$$\begin{aligned}
C'^{4\lambda'}_{9,\ell} = -C'^{4\lambda'}_{10,\ell} = -\frac{\sqrt{2}\pi^2 i}{2G_F\eta_t e^2}\big(&\tilde{\lambda}'_{\ell ij}\tilde{\lambda}'^*_{\ell ij'}\lambda'^{\mathcal{N}}_{vj2}\lambda'^{\mathcal{N}*}_{vj'3}D_2[m_{\nu_v}, m_{u_i}, m_{\tilde{d}_{Lj}}, m_{\tilde{d}_{Lj'}}] \\
&- \tilde{\lambda}'_{\ell j'k}\tilde{\lambda}'^k_{\ell jk}\tilde{\lambda}'_{ij2}\lambda'^*_{ij'3}(D_2[m_{l_i}, m_{\tilde{u}_{Lj}}, m_{\tilde{u}_{Lj'}}, m_{d_k}] + D_2[m_{\tilde{l}_{Li}}, m_{u_j}, m_{u_{j'}}, m_{\tilde{d}_{Rk}}])\big).
\end{aligned} \quad \text{(A6)}$$

The contributions of neutralino box diagrams only contain RH-quark-current parts, which are given by

$$C'^{\chi^0}_{9,\ell} = -C'^{\chi^0}_{10,\ell} = -\frac{\sqrt{2}\pi^2 i}{2G_F\eta_t e^2}\Bigg(\frac{1}{2}\Bigg(g_1 N_{n1} + g_2 N_{n2})^2 \tilde{\lambda}'_{\ell i2}\lambda'^*_{\ell i3} D_2[m_{\tilde{l}_{L\ell}}, m_{\tilde{l}_{L\ell}}, m_{u_i}, m_{\chi^0_n}]$$
$$+\frac{2}{9}g_1^2|N_{n1}|^2\tilde{\lambda}'_{\ell i2}\lambda'^*_{\ell i3}D_2[m_{u_i}, m_{\chi^0_n}, m_{\tilde{s}_R}, m_{\tilde{b}_R}]$$
$$-\frac{1}{3}N_{n1}g_1(g_1 N_{n1} + g_2 N_{n2})\tilde{\lambda}'_{\ell i2}\lambda'^*_{\ell i3}(D_2[m_{\tilde{l}_{L\ell}}, m_{u_i}, m_{\chi^0_n}, m_{\tilde{s}_R}] + D_2[m_{\tilde{l}_{L\ell}}, m_{u_i}, m_{\chi^0_n}, m_{\tilde{b}_R}]\Bigg)\Bigg). \quad \text{(A7)}$$

[1] R. Aaij *et al.* (LHCb Collaboration), Test of lepton universality in beauty-quark decays, arXiv:2103.11769.

[2] R. Aaij *et al.* (LHCb Collaboration), Search for Lepton-Universality Violation in $B^+ \to K^+\ell^+\ell^-$ Decays, Phys. Rev. Lett. **122**, 191801 (2019).

[3] R. Aaij *et al.* (LHCb Collaboration), Test of lepton universality with $B^0 \to K^{*0}\ell^+\ell^-$ decays, J. High Energy Phys. 08 (2017) 055.

[4] S. Choudhury *et al.* (BELLE Collaboration), Test of lepton flavor universality and search for lepton flavor violation in $B \to K\ell\ell$ decays, J. High Energy Phys. 03 (2021) 105.

[5] A. Abdesselam *et al.* (Belle Collaboration), Test of Lepton-Flavor Universality in $B \to K^*\ell^+\ell^-$ Decays at Belle, Phys. Rev. Lett. **126**, 161801 (2021).

[6] R. Aaij *et al.* (LHCb Collaboration), Measurement of *CP*-Averaged Observables in the $B^0 \to K^{*0}\mu^+\mu^-$ Decay, Phys. Rev. Lett. **125**, 011802 (2020).

[7] R. Aaij *et al.* (LHCb Collaboration), Angular analysis of the $B^0 \to K^{*0}\mu^+\mu^-$ decay using 3 fb^{-1} of integrated luminosity, J. High Energy Phys. 02 (2016) 104.

[8] R. Aaij *et al.* (LHCb Collaboration), Measurement of Form-Factor-Independent Observables in the Decay $B^0 \to K^{*0}\mu^+\mu^-$, Phys. Rev. Lett. **111**, 191801 (2013).

[9] V. Khachatryan *et al.* (CMS Collaboration), Angular analysis of the decay $B^0 \to K^{*0}\mu^+\mu^-$ from pp collisions at $\sqrt{s} = 8$ TeV, Phys. Lett. B **753**, 424 (2016).

[10] M. Aaboud *et al.* (ATLAS Collaboration), Angular analysis of $B^0_d \to K^*\mu^+\mu^-$ decays in pp collisions at $\sqrt{s} = 8$ TeV with the ATLAS detector, J. High Energy Phys. 10 (2018) 047.

[11] S. Wehle *et al.* (Belle Collaboration), Lepton-Flavor-Dependent Angular Analysis of $B \to K^*\ell^+\ell^-$, Phys. Rev. Lett. **118**, 111801 (2017).

[12] A. Abdesselam *et al.* (Belle Collaboration), Angular analysis of $B^0 \to K^*(892)^0\ell^+\ell^-$, in *Proceedings of the LHCSki 2016—A First Discussion of 13 TeV Results: Obergurgl, Austria, 2016* (2016).

[13] J. Aebischer, W. Altmannshofer, D. Guadagnoli, M. Reboud, P. Stangl, and D. M. Straub, *B*-decay discrepancies after Moriond 2019, Eur. Phys. J. C **80**, 252 (2020).

[14] A. K. Alok, A. Dighe, S. Gangal, and D. Kumar, Continuing search for new physics in $b \to s\mu\mu$ decays: Two operators at a time, J. High Energy Phys. 06 (2019) 089.

[15] M. Algueró, B. Capdevila, A. Crivellin, S. Descotes-Genon, P. Masjuan, J. Matias, and J. Virto, Emerging patterns of New Physics with and without Lepton Flavour Universal contributions, Eur. Phys. J. C **79**, 714 (2019).

[16] M. Ciuchini, A. M. Coutinho, M. Fedele, E. Franco, A. Paul, L. Silvestrini, and M. Valli, New Physics in $b \to s\ell^+\ell^-$ confronts new data on Lepton Universality, Eur. Phys. J. C **79**, 719 (2019).

[17] A. Arbey, T. Hurth, F. Mahmoudi, D. M. Santos, and S. Neshatpour, Update on the $b \to s$ anomalies, Phys. Rev. D **100**, 015045 (2019).

[18] K. Kowalska, D. Kumar, and E. M. Sessolo, Implications for new physics in $b \to s\mu\mu$ transitions after recent measurements by Belle and LHCb, Eur. Phys. J. C **79**, 840 (2019).

[19] B. Capdevila, U. Laa, and G. Valencia, Fitting in or odd one out? Pulls vs residual responses in $b \to s\ell^+\ell^-$, arXiv:1908.03338.

[20] S. Bhattacharya, A. Biswas, S. Nandi, and S. K. Patra, Exhaustive model selection in $b \to s\ell\ell$ decays: Pitting cross-validation against the Akaike information criterion, Phys. Rev. D **101**, 055025 (2020).

[21] F. M. Bhutta, Z.-R. Huang, C.-D. Lü, M. A. Paracha, and W. Wang, New physics in $b \to s\ell\ell$ anomalies and its implications for the complementary neutral current decays, arXiv:2009.03588.

[22] A. Biswas, S. Nandi, S. K. Patra, and I. Ray, New physics in $b \to s\ell\ell$ decays with complex Wilson coefficients, Nucl. Phys. **B969**, 115479 (2021).

[23] J. Alda, J. Guasch, and S. Peñaranda, Anomalies in B mesons decays: A phenomenological approach, arXiv: 2012.14799.

[24] A. Carvunis, F. Dettori, S. Gangal, D. Guadagnoli, and C. Normand, On the effective lifetime of $B_s \to \mu\mu\gamma$, arXiv: 2102.13390.

[25] L.-S. Geng, B. Grinstein, S. Jäger, S.-Y. Li, J. M. Camalich, and R.-X. Shi, Implications of new evidence

for lepton-universality violation in $b \to s\ell^+\ell^-$ decays, Phys. Rev. D **104**, 035029 (2021).
[26] S.-Y. Li, R.-X. Shi, and L.-S. Geng, Possible strategy of discriminating 1D new physics solutions in $b \to s\ell\ell$ decays after Moriond 2021, arXiv:2105.06768.
[27] A. Angelescu, D. Bečirević, D. A. Faroughy, F. Jaffredo, and O. Sumensari, Single leptoquark solutions to the B-physics anomalies, Phys. Rev. D **104**, 055017 (2021).
[28] W. Altmannshofer and P. Stangl, New physics in rare B decays after Moriond 2021, Eur. Phys. J. C **81**, 952 (2021).
[29] C. Cornella, D. A. Faroughy, J. Fuentes-Martin, G. Isidori, and M. Neubert, Reading the footprints of the B-meson flavor anomalies, J. High Energy Phys. 08 (2021) 050.
[30] J. Kriewald, C. Hati, J. Orloff, and A. M. Teixeira, Leptoquarks facing flavour tests and $b \to s\ell\ell$ after Moriond 2021, in *Proceedings of the 55th Rencontres de Moriond on Electroweak Interactions and Unified Theories* (2021).
[31] G. Isidori, D. Lancierini, P. Owen, and N. Serra, On the significance of new physics in $b \to s\ell^+\ell^-$ decays, Phys. Lett. B **822**, 136644 (2021).
[32] M. Algueró, B. Capdevila, S. Descotes-Genon, J. Matias, and M. Novoa-Brunet, $b \to s\ell\ell$ global fits after Moriond 2021 results, in *Proceedings of the 55th Rencontres de Moriond on Electroweak Interactions and Unified Theories* (2021).
[33] T. Hurth, F. Mahmoudi, D. M. Santos, and S. Neshatpour, More indications for lepton nonuniversality in $b \to s\ell^+\ell^-$, arXiv:2104.10058.
[34] P. F. Perez, C. Murgui, and A. D. Plascencia, Leptoquarks and matter unification: Flavor anomalies and the muon $g-2$, Phys. Rev. D **104**, 035041 (2021).
[35] J. Alda, J. Guasch, and S. Penaranda, Anomalies in B mesons decays: Present status and future collider prospects, in *Proceedings of the International Workshop on Future Linear Colliders*, edited by J. E. Brau (SLAC, eConf C2103151, 2021).
[36] R. Bause, H. Gisbert, M. Golz, and G. Hiller, Interplay of dineutrino modes with semileptonic rare B-decays, arXiv:2109.01675.
[37] R. Aaij *et al.* (LHCb Collaboration), Angular Analysis of the $B^+ \to K^{*+}\mu^+\mu^-$ Decay, Phys. Rev. Lett. **126**, 161802 (2021).
[38] R. Aaij *et al.* (LHCb Collaboration), Branching Fraction Measurements of the Rare $B_s^0 \to \phi\mu^+\mu^-$ and $B_s^0 \to f_2'(1525)\mu^+\mu^-$ Decays, Phys. Rev. Lett. **127**, 151801 (2021).
[39] R. Aaij *et al.* (LHCb Collaboration), Angular analysis and differential branching fraction of the decay $B_s^0 \to \phi\mu^+\mu^-$, J. High Energy Phys. 09 (2015) 179.
[40] A. M. Sirunyan *et al.* (CMS Collaboration), Measurement of properties of $B_s^0 \to \mu^+\mu^-$ decays and search for $B^0 \to \mu^+\mu^-$ with the CMS experiment, J. High Energy Phys. 04 (2020) 188.
[41] R. Aaij *et al.* (LHCb Collaboration), Measurement of the $B_s^0 \to \mu^+\mu^-$ decay properties and search for the $B^0 \to \mu^+\mu^-$ and $B_s^0 \to \mu^+\mu^-\gamma$ decays, arXiv:2108.09283.
[42] R. Aaij *et al.* (LHCb Collaboration), Analysis of neutral B-meson decays into two muons, arXiv:2108.09284.
[43] N. G. Deshpande and X.-G. He, Consequences of R-parity violating interactions for anomalies in $\bar{B} \to D^{(*)}\tau\bar{\nu}$ and $b \to s\mu^+\mu^-$, Eur. Phys. J. C **77**, 134 (2017).
[44] D. Das, C. Hati, G. Kumar, and N. Mahajan, Scrutinizing R-parity violating interactions in light of $R_{K^{(*)}}$ data, Phys. Rev. D **96**, 095033 (2017).
[45] K. Earl and T. Grégoire, Contributions to $b \to s\ell\ell$ anomalies from R-parity violating interactions, J. High Energy Phys. 08 (2018) 201.
[46] Q.-Y. Hu and L.-L. Huang, Explaining $b \to s\ell^+\ell^-$ data by sneutrinos in the R-parity violating MSSM, Phys. Rev. D **101**, 035030 (2020).
[47] Q.-Y. Hu, Y.-D. Yang, and M.-D. Zheng, Revisiting the B-physics anomalies in R-parity violating MSSM, Eur. Phys. J. C **80**, 365 (2020).
[48] W. Altmannshofer, P. B. Dev, A. Soni, and Y. Sui, Addressing $\mathrm{R}_{D^{(*)}}$, $\mathrm{R}_{K^{(*)}}$, muon $g-2$ and ANITA anomalies in a minimal R-parity violating supersymmetric framework, Phys. Rev. D **102**, 015031 (2020).
[49] P. Minkowski, $\mu \to e\gamma$ at a rate of one out of 10^9 muon decays?, Phys. Lett. **67B**, 421 (1977).
[50] *Proceedings of the Workshop on the Unified Theories and the Baryon Number in the Universe*, Tsukuba, Japan, 1979, edited by O. Sawada and A. Sugamoto (National Laboratory for High Energy Physics, Tsukuba, Japan, 1979).
[51] M. Gell-Mann, P. Ramond, and R. Slansky, Complex spinors and unified theories, Conf. Proc. C **790927**, 315 (1979).
[52] R. N. Mohapatra and G. Senjanovic, Neutrino Mass and Spontaneous Parity Nonconservation, Phys. Rev. Lett. **44**, 912 (1980).
[53] J. Schechter and J. W. F. Valle, Neutrino masses in $\mathrm{SU}(2) \times \mathrm{U}(1)$ theories, Phys. Rev. D **22**, 2227 (1980).
[54] J. Schechter and J. W. F. Valle, Neutrino decay and spontaneous violation of lepton number, Phys. Rev. D **25**, 774 (1982).
[55] G. Lazarides, Q. Shafi, and C. Wetterich, Proton lifetime and fermion masses in an SO(10) model, Nucl. Phys. **B181**, 287 (1981).
[56] S. Khalil, Explaining the R_K and R_{K^*} anomalies with right-handed sneutrino, J. Phys. G **45**, 125004 (2018).
[57] S.-P. Li, X.-Q. Li, Y.-D. Yang, and X. Zhang, $R_{D^{(*)}}$, $R_{K^{(*)}}$ and neutrino mass in the 2HDM-III with right-handed neutrinos, J. High Energy Phys. 09 (2018) 149.
[58] L. Delle Rose, S. Khalil, S. J. D. King, and S. Moretti, R_K and R_{K^*} in an aligned 2HDM with right-handed neutrinos, Phys. Rev. D **101**, 115009 (2020).
[59] L. T. Hue, A. B. Arbuzov, N. T. K. Ngan, and H. N. Long, Probing neutrino and Higgs sectors in $SU(2)_1 \times SU(2)_2 \times U(1)_Y$ model with lepton-flavor non-universality, Eur. Phys. J. C **77**, 346 (2017).
[60] D. Bhatia, S. Chakraborty, and A. Dighe, Neutrino mixing and R_K anomaly in $\mathrm{U}(1)_X$ models: A bottom-up approach, J. High Energy Phys. 03 (2017) 117.
[61] P. Ko, T. Nomura, and H. Okada, A flavor dependent gauge symmetry, predictive radiative seesaw and LHCb anomalies, Phys. Lett. B **772**, 547 (2017).
[62] D. N. Dinh, L. Merlo, S. T. Petcov, and R. Vega-Álvarez, Revisiting minimal lepton flavour violation in the light of leptonic CP violation, J. High Energy Phys. 07 (2017) 089.

[63] C.-W. Chiang, X.-G. He, J. Tandean, and X.-B. Yuan, $R_{K^{(*)}}$ and related $b \to s\ell\bar{\ell}$ anomalies in minimal flavor violation framework with Z' boson, Phys. Rev. D **96**, 115022 (2017).

[64] S. Antusch, C. Hohl, S. F. King, and V. Susic, Non-universal Z' from SO(10) GUTs with vector-like family and the origin of neutrino masses, Nucl. Phys. **B934**, 578 (2018).

[65] S. F. King, $R_{K^{(*)}}$ and the origin of Yukawa couplings, J. High Energy Phys. 09 (2018) 069.

[66] J. Heeck and D. Teresi, Pati-Salam explanations of the B-meson anomalies, J. High Energy Phys. 12 (2018) 103.

[67] D. Borah, L. Mukherjee, and S. Nandi, Low scale $\mathrm{U}(1)_X$ gauge symmetry as an origin of dark matter, neutrino mass and flavour anomalies, J. High Energy Phys. 12 (2020) 052.

[68] J.-Y. Cen, Y. Cheng, X.-G. He, and J. Sun, Flavor specific $U(1)_{B_q-L_\mu}$ gauge model for muon $g-2$ and $b \to s\bar{\mu}\mu$ anomalies, arXiv:2104.05006.

[69] J. S. Alvarado, S. F. Mantilla, R. Martinez, and F. Ochoa, A non-universal $U(1)_X$ extension to the Standard Model to study the B meson anomaly and muon $g-2$, arXiv:2105.04715.

[70] B. Dutta, S. Ghosh, P. Huang, and J. Kumar, Explaining $g_\mu - 2$ and $R_{K^{(*)}}$ using the light mediators of $U(1)_{T3R}$, arXiv:2105.07655.

[71] A. Greljo, P. Stangl, and A. E. Thomsen, A model of muon anomalies, Phys. Lett. B **820**, 136554 (2021).

[72] A. Greljo, Y. Soreq, P. Stangl, A. E. Thomsen, and J. Zupan, Muonic force behind flavor anomalies, arXiv:2107.07518.

[73] D. Bhatia, N. Desai, and A. Dighe, Frugal $U(1)_X$ models with non-minimal flavor violation for $b \to s\ell\ell$ anomalies and neutrino mixing, arXiv:2109.07093.

[74] I. Esteban, M. Gonzalez-Garcia, M. Maltoni, T. Schwetz, and A. Zhou, The fate of hints: Updated global analysis of three-flavor neutrino oscillations, J. High Energy Phys. 09 (2020) 178.

[75] R. N. Mohapatra, Mechanism for Understanding Small Neutrino Mass in Superstring Theories, Phys. Rev. Lett. **56**, 561 (1986).

[76] R. N. Mohapatra and J. W. F. Valle, Neutrino mass and baryon number nonconservation in superstring models, Phys. Rev. D **34**, 1642 (1986).

[77] N. Escudero, D. E. Lopez-Fogliani, C. Munoz, and R. Ruiz de Austri, Analysis of the parameter space and spectrum of the mu nu SSM, J. High Energy Phys. 12 (2008) 099.

[78] J. Fidalgo and C. Munoz, The $\mu\nu$SSM with an extra U(1), J. High Energy Phys. 04 (2012) 090.

[79] D. E. Lopez-Fogliani and C. Munoz, On a reinterpretation of the Higgs field in supersymmetry and a proposal for new quarks, Phys. Lett. B **771**, 136 (2017).

[80] J. P. Lees *et al.* (*BABAR* Collaboration), Evidence for an Excess of $\bar{B} \to D^{(*)}\tau^-\bar{\nu}_\tau$ Decays, Phys. Rev. Lett. **109**, 101802 (2012).

[81] J. P. Lees *et al.* (*BABAR* Collaboration), Measurement of an excess of $\bar{B} \to D^{(*)}\tau^-\bar{\nu}_\tau$ decays and implications for charged Higgs bosons, Phys. Rev. D **88**, 072012 (2013).

[82] M. Huschle *et al.* (Belle Collaboration), Measurement of the branching ratio of $\bar{B} \to D^{(*)}\tau^-\bar{\nu}_\tau$ relative to $\bar{B} \to D^{(*)}\ell^-\bar{\nu}_\ell$ decays with hadronic tagging at Belle, Phys. Rev. D **92**, 072014 (2015).

[83] S. Hirose *et al.* (Belle Collaboration), Measurement of the τ Lepton Polarization and $R(D^*)$ in the Decay $\bar{B} \to D^*\tau^-\bar{\nu}_\tau$, Phys. Rev. Lett. **118**, 211801 (2017).

[84] S. Hirose *et al.* (Belle Collaboration), Measurement of the τ lepton polarization and $R(D^*)$ in the decay $\bar{B} \to D^*\tau^-\bar{\nu}_\tau$ with one-prong hadronic τ decays at Belle, Phys. Rev. D **97**, 012004 (2018).

[85] G. Caria *et al.* (Belle Collaboration), Measurement of $\mathcal{R}(D)$ and $\mathcal{R}(D^*)$ with a Semileptonic Tagging Method, Phys. Rev. Lett. **124**, 161803 (2020).

[86] R. Aaij *et al.* (LHCb Collaboration), Measurement of the Ratio of Branching Fractions $\mathcal{B}(\bar{B}^0 \to D^{*+}\tau^-\bar{\nu}_\tau)/\mathcal{B}(\bar{B}^0 \to D^{*+}\mu^-\bar{\nu}_\mu)$, Phys. Rev. Lett. **115**, 111803 (2015); **115**, 159901(E) (2015).

[87] R. Aaij *et al.* (LHCb Collaboration), Measurement of the Ratio of the $B^0 \to D^{*-}\tau^+\nu_\tau$ and $B^0 \to D^{*-}\mu^+\nu_\mu$ Branching Fractions Using Three-Prong τ-Lepton Decays, Phys. Rev. Lett. **120**, 171802 (2018).

[88] R. Aaij *et al.* (LHCb Collaboration), Test of Lepton Flavor Universality by the measurement of the $B^0 \to D^{*-}\tau^+\nu_\tau$ branching fraction using three-prong τ decays, Phys. Rev. D **97**, 072013 (2018).

[89] Y. S. Amhis *et al.* (HFLAV Collaboration), Averages of b-hadron, c-hadron, and τ-lepton properties as of 2018, Eur. Phys. J. C **81**, 226 (2021).

[90] D. Bigi and P. Gambino, Revisiting $B \to D\ell\nu$, Phys. Rev. D **94**, 094008 (2016).

[91] F. U. Bernlochner, Z. Ligeti, M. Papucci, and D. J. Robinson, Combined analysis of semileptonic B decays to D and D^*: $R(D^{(*)})$, $|V_{cb}|$, and new physics, Phys. Rev. D **95**, 115008 (2017); **97**, 059902(E) (2018).

[92] D. Bigi, P. Gambino, and S. Schacht, $R(D^*)$, $|V_{cb}|$, and the heavy quark symmetry relations between form factors, J. High Energy Phys. 11 (2017) 061.

[93] S. Jaiswal, S. Nandi, and S. K. Patra, Extraction of $|V_{cb}|$ from $B \to D^{(*)}\ell\nu_\ell$ and the Standard Model predictions of $R(D^{(*)})$, J. High Energy Phys. 12 (2017) 060.

[94] P. Gambino, M. Jung, and S. Schacht, The V_{cb} puzzle: An update, Phys. Lett. B **795**, 386 (2019).

[95] M. Bordone, M. Jung, and D. van Dyk, Theory determination of $\bar{B} \to D^{(*)}\ell^-\bar{\nu}$ form factors at $\mathcal{O}(1/m_c^2)$, Eur. Phys. J. C **80**, 74 (2020).

[96] S. Jaiswal, S. Nandi, and S. K. Patra, Updates on extraction of $|V_{cb}|$ and SM prediction of R(D*) in $B \to D^*\ell\nu_\ell$ decays, J. High Energy Phys. 06 (2020) 165.

[97] K. Cheung, Z.-R. Huang, H.-D. Li, C.-D. Lü, Y.-N. Mao, and R.-Y. Tang, Revisit to the $b \to c\tau\nu$ transition: In and beyond the SM, Nucl. Phys. **B965**, 115354 (2021).

[98] H.-M. Choi, Self-consistent light-front quark model analysis of $B \to D\ell\nu_\ell$ transition form factors, Phys. Rev. D **103**, 073004 (2021).

[99] S. Iguro and R. Watanabe, Bayesian fit analysis to full distribution data of $\mathrm{\bar{B}} \to \mathrm{D}^{(*)}\ell\bar{\nu}: |\mathrm{V_{cb}}|$ determination and new physics constraints, J. High Energy Phys. 08 (2020) 006.

[100] K. Hara, $R(D)$ and $R(D^*)$ at Belle, Proc. Sci., 377 (**2020**) 041.

[101] B. Abi *et al.* (Muon $g-2$ Collaboration), Measurement of the Positive Muon Anomalous Magnetic Moment to 0.46 ppm, Phys. Rev. Lett. **126**, 141801 (2021).
[102] T. Albahri *et al.* (Muon $g-2$ Collaboration), Measurement of the anomalous precession frequency of the muon in the Fermilab Muon $g-2$ experiment, Phys. Rev. D **103**, 072002 (2021).
[103] T. Albahri *et al.* (Muon $g-2$ Collaboration), Magnetic field measurement and analysis for the Muon $g-2$ Experiment at Fermilab, Phys. Rev. A **103**, 042208 (2021).
[104] T. Aoyama *et al.*, The anomalous magnetic moment of the muon in the Standard Model, Phys. Rep. **887**, 1 (2020).
[105] S. Borsanyi *et al.*, Leading hadronic contribution to the muon magnetic moment from lattice QCD, Nature (London) **593**, 51 (2021).
[106] G. Colangelo, M. Hoferichter, and P. Stoffer, Two-pion contribution to hadronic vacuum polarization, J. High Energy Phys. 02 (2019) 006.
[107] M. Davier, A. Hoecker, B. Malaescu, and Z. Zhang, A new evaluation of the hadronic vacuum polarisation contributions to the muon anomalous magnetic moment and to $\alpha(m_Z^2)$, Eur. Phys. J. C **80**, 241 (2020); **80**, 410(E) (2020).
[108] A. Keshavarzi, D. Nomura, and T. Teubner, $g-2$ of charged leptons, $\alpha(M_Z^2)$, and the hyperfine splitting of muonium, Phys. Rev. D **101**, 014029 (2020).
[109] M. Hoferichter, B.-L. Hoid, and B. Kubis, Three-pion contribution to hadronic vacuum polarization, J. High Energy Phys. 08 (2019) 137.
[110] A. Crivellin, M. Hoferichter, C. A. Manzari, and M. Montull, Hadronic Vacuum Polarization: $(g-2)_\mu$ Versus Global Electroweak Fits, Phys. Rev. Lett. **125**, 091801 (2020).
[111] A. Keshavarzi, W. J. Marciano, M. Passera, and A. Sirlin, Muon $g-2$ and $\Delta\alpha$ connection, Phys. Rev. D **102**, 033002 (2020).
[112] E. de Rafael, Constraints between $\Delta\alpha_{\rm had}(M_Z^2)$ and $(g_\mu-2)_{\rm HVP}$, Phys. Rev. D **102**, 056025 (2020).
[113] B. Malaescu and M. Schott, Impact of correlations between a_μ and $\alpha_{\rm QED}$ on the EW fit, Eur. Phys. J. C **81**, 46 (2021).
[114] G. W. Bennett *et al.* (Muon $g-2$ Collaboration), Final report of the muon E821 anomalous magnetic moment measurement at BNL, Phys. Rev. D **73**, 072003 (2006).
[115] D. Hanneke, S. F. Hoogerheide, and G. Gabrielse, Cavity control of a single-electron quantum cyclotron: Measuring the electron magnetic moment, Phys. Rev. A **83**, 052122 (2011).
[116] T. Aoyama, T. Kinoshita, and M. Nio, Revised and improved value of the QED tenth-order electron anomalous magnetic moment, Phys. Rev. D **97**, 036001 (2018).
[117] R. H. Parker, C. Yu, W. Zhong, B. Estey, and H. Müller, Measurement of the fine-structure constant as a test of the Standard Model, Science **360**, 191 (2018).
[118] L. Morel, Z. Yao, P. Cladé, and S. Guellati-Khélifa, Determination of the fine-structure constant with an accuracy of 81 parts per trillion, Nature (London) **588**, 61 (2020).
[119] A. Gérardin, The anomalous magnetic moment of the muon: Status of lattice QCD calculations, Eur. Phys. J. A **57**, 116 (2021).
[120] J. Hisano and K. Tobe, Neutrino masses, muon $g-2$, and lepton flavor violation in the supersymmetric seesaw model, Phys. Lett. B **510**, 197 (2001).
[121] J. E. Kim, B. Kyae, and H. M. Lee, Effective supersymmetric theory and $(g-2)$(muon with R-parity violation), Phys. Lett. B **520**, 298 (2001).
[122] S. P. Martin and J. D. Wells, Muon anomalous magnetic dipole moment in supersymmetric theories, Phys. Rev. D **64**, 035003 (2001).
[123] D. Stockinger, The muon magnetic moment and supersymmetry, J. Phys. G **34**, R45 (2007).
[124] A. S. Belyaev, J. E. Camargo-Molina, S. F. King, D. J. Miller, A. P. Morais, and P. B. Schaefers, A to Z of the muon anomalous magnetic moment in the MSSM with Pati-Salam at the GUT scale, J. High Energy Phys. 06 (2016) 142.
[125] M. Yamaguchi and W. Yin, A novel approach to finely tuned supersymmetric standard models: The case of the non-universal Higgs mass model, Prog. Theor. Exp. Phys. **2018**, 023B06 (2018).
[126] A. Choudhury, L. Darmé, L. Roszkowski, E. M. Sessolo, and S. Trojanowski, Muon $g-2$ and related phenomenology in constrained vector-like extensions of the MSSM, J. High Energy Phys. 05 (2017) 072.
[127] A. Choudhury, S. Rao, and L. Roszkowski, Impact of LHC data on muon $g-2$ solutions in a vectorlike extension of the constrained MSSM, Phys. Rev. D **96**, 075046 (2017).
[128] Z. Altın, O. Özdal, and C. S. Un, Muon $g-2$ in an alternative quasi-Yukawa unification with a less fine-tuned seesaw mechanism, Phys. Rev. D **97**, 055007 (2018).
[129] W. Kotlarski, D. Stöckinger, and H. Stöckinger-Kim, Low-energy lepton physics in the MRSSM: $(g-2)_\mu$, $\mu \to e\gamma$ and $\mu \to e$ conversion, J. High Energy Phys. 08 (2019) 082.
[130] M. Endo and W. Yin, Explaining electron and muon $g-2$ anomaly in SUSY without lepton-flavor mixings, J. High Energy Phys. 08 (2019) 122.
[131] M. Badziak and K. Sakurai, Explanation of electron and muon $g-2$ anomalies in the MSSM, J. High Energy Phys. 10 (2019) 024.
[132] E. Kpatcha, I. N. Lara, D. E. López-Fogliani, C. Muñoz, and N. Nagata, Explaining muon $g-2$ data in the $\mu\nu$SSM, Eur. Phys. J. C **81**, 154 (2021).
[133] S. Heinemeyer, E. Kpatcha, I. n. Lara, D. E. López-Fogliani, C. Muñoz, and N. Nagata, The new $(g-2)_\mu$ result and the $\mu\nu$SSM, Eur. Phys. J. C **81**, 802 (2021).
[134] R. Nagai and N. Yokozaki, Lepton flavor violations in SUSY models for muon $g-2$ with right-handed neutrinos, J. High Energy Phys. 01 (2021) 099.
[135] W. Yin and M. Yamaguchi, Muon $g-2$ at multi-TeV muon collider, arXiv:2012.03928.
[136] J.-L. Yang, T.-F. Feng, and H.-B. Zhang, Electron and muon $(g-2)$ in the B-LSSM, J. Phys. G **47**, 055004 (2020).
[137] C. Han, M. L. López-Ibáñez, A. Melis, O. Vives, L. Wu, and J. M. Yang, LFV and $(g-2)$ in non-universal SUSY models with light higgsinos, J. High Energy Phys. 05 (2020) 102.

[138] W. Yin, Radiative lepton mass and muon $g-2$ with suppressed lepton flavor and CP violations, J. High Energy Phys. 08 (2021) 043.
[139] W. Yin, Muon $g-2$ anomaly in anomaly mediation, J. High Energy Phys. 06 (2021) 029.
[140] J. Cao, J. Lian, L. Meng, Y. Yue, and P. Zhu, Anomalous muon magnetic moment in the inverse seesaw extended next-to-minimal supersymmetric standard model, Phys. Rev. D **101**, 095009 (2020).
[141] J. Cao, Y. He, J. Lian, D. Zhang, and P. Zhu, Electron and muon anomalous magnetic moments in the inverse seesaw extended NMSSM, Phys. Rev. D **104**, 055009 (2021).
[142] J. Cao, J. Lian, Y. Pan, D. Zhang, and P. Zhu, Imporved $(g-2)_\mu$ measurement and singlino dark matter in the general NMSSM, J. High Energy Phys. 09 (2021) 175.
[143] H.-B. Zhang, C.-X. Liu, J.-L. Yang, and T.-F. Feng, Muon anomalous magnetic dipole moment in the $\mu\nu$SSM, arXiv:2104.03489.
[144] M. Endo, K. Hamaguchi, S. Iwamoto, and T. Kitahara, Supersymmetric interpretation of the muon $g-2$ anomaly, J. High Energy Phys. 07 (2021) 075.
[145] W. Ahmed, I. Khan, J. Li, T. Li, S. Raza, and W. Zhang, The natural explanation of the muon anomalous magnetic moment via the electroweak supersymmetry from the GmSUGRA in the MSSM, arXiv:2104.03491.
[146] S. Baum, M. Carena, N. R. Shah, and C. E. M. Wagner, The tiny $(g-2)$ muon wobble from small-μ supersymmetry, arXiv:2104.03302.
[147] M. Abdughani, Y.-Z. Fan, L. Feng, Y.-L. S. Tsai, L. Wu, and Q. Yuan, A common origin of muon $g-2$ anomaly, Galaxy Center GeV excess and AMS-02 anti-proton excess in the NMSSM, Sci. Bull. **66**, 2170 (2021).
[148] M. Ibe, S. Kobayashi, Y. Nakayama, and S. Shirai, Muon $g-2$ in gauge mediation without SUSY CP problem, J. High Energy Phys. 07 (2021) 098.
[149] M. Van Beekveld, W. Beenakker, M. Schutten, and J. De Wit, Dark matter, fine-tuning and $(g-2)_\mu$ in the pMSSM, SciPost Phys. **11**, 049 (2021).
[150] P. Cox, C. Han, and T. T. Yanagida, Muon $g-2$ and co-annihilating dark matter in the MSSM, Phys. Rev. D **104**, 075035 (2021).
[151] C. Han, Muon $g-2$ and CP violation in MSSM, arXiv:2104.03292.
[152] Y. Gu, N. Liu, L. Su, and D. Wang, Heavy bino and slepton for muon $g-2$ anomaly, Nucl. Phys. **B969**, 115481 (2021).
[153] F. Wang, L. Wu, Y. Xiao, J. M. Yang, and Y. Zhang, GUT-scale constrained SUSY in light of new muon $g-2$ measurement, Nucl. Phys. **B970**, 115486 (2021).
[154] A. Aboubrahim, M. Klasen, and P. Nath, What the Fermilab muon $g-2$ experiment tells us about discovering supersymmetry at high luminosity and high energy upgrades to the LHC, Phys. Rev. D **104**, 035039 (2021).
[155] J.-L. Yang, H.-B. Zhang, C.-X. Liu, X.-X. Dong, and T.-F. Feng, Muon $(g-2)$ in the B-LSSM, J. High Energy Phys. 08 (2021) 086.
[156] P. Athron, C. Balázs, D. H. Jacob, W. Kotlarski, D. Stöckinger, and H. Stöckinger-Kim, New physics explanations of a_μ in light of the FNAL muon $g-2$ measurement, J. High Energy Phys. 09 (2021) 080.
[157] W. Altmannshofer, S. A. Gadam, S. Gori, and N. Hamer, Explaining $(g-2)_\mu$ with multi-TeV sleptons, J. High Energy Phys. 07 (2021) 118.
[158] Z.-N. Zhang, H.-B. Zhang, J.-L. Yang, S.-M. Zhao, and T.-F. Feng, Higgs boson decays with lepton flavor violation in the $B-L$ symmetric SSM, Phys. Rev. D **103**, 115015 (2021).
[159] Z. Li, G.-L. Liu, F. Wang, J. M. Yang, and Y. Zhang, Gluino-SUGRA scenarios in light of FNAL muon $g-2$ anomaly, arXiv:2106.04466.
[160] P. S. B. Dev, A. Soni, and F. Xu, Hints of natural supersymmetry in flavor anomalies?, arXiv:2106.15647.
[161] J. S. Kim, D. E. Lopez-Fogliani, A. D. Perez, and R. R. de Austri, The new $(g-2)_\mu$ and right-handed sneutrino dark matter, arXiv:2107.02285.
[162] J. Ellis, J. L. Evans, N. Nagata, D. V. Nanopoulos, and K. A. Olive, Flipped $g_\mu-2$, arXiv:2107.03025.
[163] S.-M. Zhao, L.-H. Su, X.-X. Dong, T.-T. Wang, and T.-F. Feng, Study muon $g-2$ at two loop level in the $U(1)_X$SSM, arXiv:2107.03571.
[164] M. Frank, Y. Hiçyılmaz, S. Mondal, O. Özdal, and C. S. Ün, Electron and muon magnetic moments and implications for dark matter and model characterisation in non-universal $U(1)'$ supersymmetric models, J. High Energy Phys. 10 (2021) 063.
[165] S. Li, Y. Xiao, and J. M. Yang, Can electron and muon $g-2$ anomalies be jointly explained in SUSY?, arXiv:2107.04962.
[166] A. Aboubrahim, M. Klasen, P. Nath, and R. M. Syed, Future searches for SUSY at the LHC post Fermilab $(g-2)_\mu$, arXiv:2107.06021.
[167] Y. Nakai, M. Reece, and M. Suzuki, Supersymmetric alignment models for $(g-2)_\mu$, J. High Energy Phys. 10 (2021) 068.
[168] S. Li, Y. Xiao, and J. M. Yang, Constraining CP-phases in SUSY: An interplay of muon/electron $g-2$ and electron EDM, arXiv:2108.00359.
[169] W. Ke and P. Slavich, Higgs-mass constraints on a supersymmetric solution of the muon $g-2$ anomaly, arXiv:2109.15277.
[170] J. Rosiek, Complete set of Feynman rules for the minimal supersymmetric extension of the standard model, Phys. Rev. D **41**, 3464 (1990).
[171] J. Rosiek, Complete set of Feynman rules for the MSSM: Erratum, Phys. Rev. D **41**, 3464 (1990).
[172] S. Weinberg, Supersymmetry at ordinary energies. 1. Masses and conservation laws, Phys. Rev. D **26** (1982) 287.
[173] N. Sakai and T. Yanagida, Proton decay in a class of supersymmetric grand unified models, Nucl. Phys. **B197**, 533 (1982).
[174] T. Aaltonen *et al.* (CDF Collaboration), Search for R-Parity Violating Decays of τ Sneutrinos to $e\mu$, $\mu\tau$, and $e\tau$ Pairs in $p\bar{p}$ Collisions at $\sqrt{s}=1.96$ TeV, Phys. Rev. Lett. **105**, 191801 (2010).
[175] V. M. Abazov *et al.* (D0 Collaboration), Search for Sneutrino Production in $e\mu$ Final States in 5.3 fb^{-1} of $p\bar{p}$ Collisions at $\sqrt{s}=1.96$ TeV, Phys. Rev. Lett. **105**, 191802 (2010).
[176] G. Aad *et al.* (ATLAS Collaboration), Search for a Heavy Neutral Particle Decaying to $e\mu$, $e\tau$, or $\mu\tau$ in pp Collisions

at $\sqrt{s} = 8$ TeV with the ATLAS Detector, Phys. Rev. Lett. **115**, 031801 (2015).

[177] V. Khachatryan *et al.* (CMS Collaboration), Search for lepton flavour violating decays of heavy resonances and quantum black holes to an eμ pair in proton-proton collisions at $\sqrt{s} = 8$ TeV, Eur. Phys. J. C **76**, 317 (2016).

[178] M. Aaboud *et al.* (ATLAS Collaboration), Search for new phenomena in different-flavour high-mass dilepton final states in pp collisions at $\sqrt{s} = 13$ Tev with the ATLAS detector, Eur. Phys. J. C **76**, 541 (2016).

[179] M. Aaboud *et al.* (ATLAS Collaboration), Search for lepton-flavor violation in different-flavor, high-mass final states in pp collisions at $\sqrt{s} = 13$ TeV with the ATLAS detector, Phys. Rev. D **98**, 092008 (2018).

[180] A. M. Sirunyan *et al.* (CMS Collaboration), Search for lepton-flavor violating decays of heavy resonances and quantum black holes to eμ final states in proton-proton collisions at $\sqrt{s} = 13$ TeV, J. High Energy Phys. 04 (2018) 073.

[181] B. Le (ATLAS Collaboration), Search for lepton flavour violation with the ATLAS experiment, SciPost Phys. Proc. **1**, 020 (2019).

[182] M. Aaboud *et al.* (ATLAS Collaboration), Search for supersymmetry in events with four or more leptons in $\sqrt{s} = 13$ TeV pp collisions with ATLAS, Phys. Rev. D **98**, 032009 (2018).

[183] M. Aaboud *et al.* (ATLAS Collaboration), Search for lepton-flavor violation in different-flavor, high-mass final states in pp collisions at $\sqrt{s} = 13$ TeV with the ATLAS detector, Phys. Rev. D **98**, 092008 (2018).

[184] G. Aad *et al.* (ATLAS Collaboration), Search for supersymmetry in events with four or more charged leptons in 139 fb^{-1} of $\sqrt{s} = 13$ TeV pp collisions with the ATLAS detector, J. High Energy Phys. 07 (2021) 167.

[185] M. Hirsch, M. A. Diaz, W. Porod, J. C. Romao, and J. W. F. Valle, Neutrino masses and mixings from supersymmetry with bilinear R parity violation: A Theory for solar and atmospheric neutrino oscillations, Phys. Rev. D **62**, 113008 (2000); **65**, 119901(E) (2002).

[186] I. Esteban, M. Gonzalez-Garcia, A. Hernandez-Cabezudo, M. Maltoni, and T. Schwetz, Global analysis of three-flavour neutrino oscillations: synergies and tensions in the determination of θ_{23}, δ_{CP}, and the mass ordering, J. High Energy Phys. 01 (2019) 106.

[187] P. B. Dev, S. Mondal, B. Mukhopadhyaya, and S. Roy, Phenomenology of light sneutrino dark matter in cMSSM/mSUGRA with inverse seesaw, J. High Energy Phys. 09 (2012) 110.

[188] J. Chang, K. Cheung, H. Ishida, C.-T. Lu, M. Spinrath, and Y.-L. S. Tsai, A supersymmetric electroweak scale seesaw model, J. High Energy Phys. 10 (2017) 039.

[189] S. Descotes-Genon, D. Ghosh, J. Matias, and M. Ramon, Exploring new physics in the C7-C7' plane, J. High Energy Phys. 06 (2011) 099.

[190] T. Moroi, The Muon anomalous magnetic dipole moment in the minimal supersymmetric standard model, Phys. Rev. D **53**, 6565 (1996); **56**, 4424(E) (1997).

[191] J. Aebischer, J. Kumar, P. Stangl, and D. M. Straub, A global likelihood for precision constraints and flavour anomalies, Eur. Phys. J. C **79**, 509 (2019).

[192] P. A. Zyla *et al.* (Particle Data Group Collaboration), Review of particle physics, Prog. Theor. Exp. Phys. **2020**, 083C01 (2020).

[193] A. J. Buras, J. Girrbach-Noe, C. Niehoff, and D. M. Straub, $B \to K^{(*)}\nu\bar{\nu}$ decays in the Standard Model and beyond, J. High Energy Phys. 02 (2015) 184.

[194] J. E. Kim, P. Ko, and D.-G. Lee, More on R-parity and lepton family number violating couplings from muon(ium) conversion, and tau and pi0 decays, Phys. Rev. D **56**, 100 (1997).

[195] B. de Carlos and P. L. White, R-parity violation and quark flavor violation, Phys. Rev. D **55**, 4222 (1997).

[196] M. Misiak *et al.*, Updated NNLO QCD Predictions for the Weak Radiative B-Meson Decays, Phys. Rev. Lett. **114**, 221801 (2015).

[197] R. Aaij *et al.* (LHCb Collaboration), Precise determination of the $B_s^0 - \bar{B}_s^0$ oscillation frequency, arXiv:2104.04421.

[198] L. Di Luzio, M. Kirk, A. Lenz, and T. Rauh, ΔM_s theory precision confronts flavour anomalies, J. High Energy Phys. 12 (2019) 009.

[199] A. Abada, M. E. Krauss, W. Porod, F. Staub, A. Vicente, and C. Weiland, Lepton flavor violation in low-scale seesaw models: SUSY and non-SUSY contributions, J. High Energy Phys. 11 (2014) 048.

[200] K. Agashe *et al.* (Top Quark Working Group Collaboration), Working group report: Top quark, in *Proceedings of the Community Summer Study 2013: Snowmass on the Mississippi* (Fermilab and SLAC, 2013).

[201] M. Aaboud *et al.* (ATLAS Collaboration), Search for flavour-changing neutral current top-quark decays $t \to qZ$ in proton-proton collisions at $\sqrt{s} = 13$ TeV with the ATLAS detector, J. High Energy Phys. 07 (2018) 176.

[202] G. Aad *et al.* (ATLAS Collaboration), Search for flavour-changing neutral currents in processes with one top quark and a photon using 81 fb^{-1} of pp collisions at $\sqrt{s} =$ 13 TeV with the ATLAS experiment, Phys. Lett. B **800**, 135082 (2020).

[203] V. Khachatryan *et al.* (CMS Collaboration), Search for anomalous Wtb couplings and flavour-changing neutral currents in t-channel single top quark production in pp collisions at $\sqrt{s} = 7$ and 8 TeV, J. High Energy Phys. 02 (2017) 028.

[204] M. Aaboud *et al.* (ATLAS Collaboration), Search for top-quark decays $t \to Hq$ with 36 fb^{-1} of pp collision data at $\sqrt{s} = 13$ TeV with the ATLAS detector, J. High Energy Phys. 05 (2019) 123.

[205] J. M. Yang, B.-L. Young, and X. Zhang, Flavor changing top quark decays in R parity violating SUSY, Phys. Rev. D **58**, 055001 (1998).

[206] G. Eilam, A. Gemintern, T. Han, J. M. Yang, and X. Zhang, Top quark rare decay $t \to$ ch in R-parity violating SUSY, Phys. Lett. B **510**, 227 (2001).

[207] G. Passarino and M. J. G. Veltman, One loop corrections for $e+$ $e-$ annihilation into mu+ mu- in the weinberg model, Nucl. Phys. **B160**, 151 (1979).

[208] M. Beneke *et al.*, Top quark physics, in *Proceedings of the Workshop on Standard Model Physics (and more) at the LHC (First Plenary Meeting)* (CERN, Geneva, 2000).
[209] M. Aaboud *et al.* (ATLAS Collaboration), Search for B-L R -parity-violating top squarks in $\sqrt{s} = 13$ TeV pp collisions with the ATLAS experiment, Phys. Rev. D **97**, 032003 (2018).
[210] A. M. Sirunyan *et al.* (CMS Collaboration), Search for long-lived particles decaying into displaced jets in proton-proton collisions at $\sqrt{s} = 13$ TeV, Phys. Rev. D **99**, 032011 (2019).
[211] M. Aaboud *et al.* (ATLAS Collaboration), Search for heavy charged long-lived particles in the ATLAS detector in 36.1 fb^{-1} of proton-proton collision data at $\sqrt{s} = 13$ TeV, Phys. Rev. D **99**, 092007 (2019).
[212] G. Aad *et al.* (ATLAS Collaboration), Search for long-lived, massive particles in events with a displaced vertex and a muon with large impact parameter in pp collisions at $\sqrt{s} = 13$ TeV with the ATLAS detector, Phys. Rev. D **102**, 032006 (2020).
[213] G. Aad *et al.* (ATLAS Collaboration), Search for R-parity violating supersymmetry in a final state containing leptons and many jets with the ATLAS experiment using $\sqrt{s} =$ 13 TeV proton-proton collision data, Eur. Phys. J. C **81**, 1023 (2021).
[214] A. M. Sirunyan *et al.* (CMS Collaboration), Search for top squark production in fully-hadronic final states in proton-proton collisions at $\sqrt{s} = 13$ TeV, Phys. Rev. D **104**, 052001 (2021).
[215] A. Tumasyan *et al.* (CMS Collaboration), Combined searches for the production of supersymmetric top quark partners in proton-proton collisions at $\sqrt{s} = 13$ TeV, Eur. Phys. J. C **81**, 970 (2021).
[216] A. M. Sirunyan *et al.* (CMS Collaboration), Search for supersymmetric partners of electrons and muons in proton-proton collisions at $\sqrt{s} = 13$ TeV, Phys. Lett. B **790**, 140 (2019).
[217] G. Aad *et al.* (ATLAS Collaboration), Search for electroweak production of charginos and sleptons decaying into final states with two leptons and missing transverse momentum in $\sqrt{s} = 13$ TeV pp collisions using the ATLAS detector, Eur. Phys. J. C **80**, 123 (2020).
[218] A. M. Sirunyan *et al.* (CMS Collaboration), Search for supersymmetry in final states with two oppositely charged same-flavor leptons and missing transverse momentum in proton-proton collisions at $\sqrt{s} = 13$ TeV, J. High Energy Phys. 04 (2021) 123.
[219] G. Aad *et al.* (ATLAS Collaboration), Searches for electroweak production of supersymmetric particles with compressed mass spectra in $\sqrt{s} = 13$ TeV pp collisions with the ATLAS detector, Phys. Rev. D **101**, 052005 (2020).
[220] J. S. Alvarado and R. Martinez, PMNS matrix in a non-universal $U(1)_X$ extension to the MSSM with one massless neutrino, arXiv:2007.14519.
[221] Summer 2019 CKMfitter updates. http://ckmfitter.in2p3.fr/.
[222] V. De Romeri, K. M. Patel, and J. W. Valle, Inverse seesaw mechanism with compact supersymmetry: Enhanced naturalness and light superpartners, Phys. Rev. D **98**, 075014 (2018).
[223] H. Khanpour, Probing top quark FCNC couplings in the triple-top signal at the high energy LHC and future circular collider, Nucl. Phys. **B958**, 115141 (2020).